



HAL
open science

The cluster fleet explores waves in the magnetosphere: Chosen illustrations

Pierrette Décréau, Philippe Louarn, Robert L. Mutel, Michel Parrot,
Jean-Louis Pinçon, A. Vaivads, Patrick Robert

► To cite this version:

Pierrette Décréau, Philippe Louarn, Robert L. Mutel, Michel Parrot, Jean-Louis Pinçon, et al.. The cluster fleet explores waves in the magnetosphere: Chosen illustrations. *Radio Science Bulletin*, 2005, 315, pp.4-21. 10.23919/URSIRSB.2005.7909703 . insu-03218936

HAL Id: insu-03218936

<https://insu.hal.science/insu-03218936>

Submitted on 6 May 2021

HAL is a multi-disciplinary open access archive for the deposit and dissemination of scientific research documents, whether they are published or not. The documents may come from teaching and research institutions in France or abroad, or from public or private research centers.

L'archive ouverte pluridisciplinaire **HAL**, est destinée au dépôt et à la diffusion de documents scientifiques de niveau recherche, publiés ou non, émanant des établissements d'enseignement et de recherche français ou étrangers, des laboratoires publics ou privés.

The Cluster Fleet Explores Waves in the Magnetosphere: Chosen Illustrations

P.M.E. Décréau
Ph. Louarn, R.L. Mutel
M. Parrot, J.-L. Pinçon
A.Vaivads, P. Robert

1. Introduction

The four-point Cluster constellation is designed to explore in 3D, locally and remotely, phenomena critical to the physics of the Earth's magnetosphere. The purpose of this paper is to illustrate the role of this pioneer mission in the field of plasma and radio waves that are of general importance in space plasma and solar terrestrial physics. We have chosen, somewhat arbitrarily, examples in published literature obtained with the four points fleet, with the objective to present a variety rather than a complete panorama of the major results obtained up to now. Moreover, the emphasis has been to present which novel features are derived from the four spacecraft observations, rather than how they are changing our views about physical processes shaping our environment. The latter would deserve full developments, but a flavor of it is given in the paper. We describe shortly the multiple point analysis tools that were necessary for deriving the results, referring to bibliography for the interested reader. Let's start with a few words of history.

1.1 The Mission

The concept of a four spacecraft fleet, toward a 3D exploration of the magnetosphere, came to life in February 1986, when ESA chose Cluster and SOHO (Solar and Heliospheric Observatory) as the first "cornerstone" in its Horizon 2000 Science Programme [1]. Such a concept had been discussed after the first space era which allowed, through single satellites explorations, to derive a general map of the space environment of the Earth [3], but where many features, in particular essential details of key interface regions, and in general most of the global dynamics, were lacking.

The Earth's magnetosphere forms, as a result of the interaction of the solar wind, a fully ionized, collisionless plasma, with the magnetic field of the Earth. In a stationary picture (see diagram in Figure 1), the magnetosphere presents various cells and their boundaries which result, not only from the solar wind/terrestrial magnetic field interaction, but also from the presence of plasma (also collisionless) formed in the ionosphere, the high altitude layers of our planet's atmosphere. Figure 1 shows the Earth's magnetic field lines and the main regions in space around the Earth. Starting from the Earth, one encounters the plasmasphere (dark orange), a region of high-density plasma that is mainly of ionospheric origin. Chorus waves, the subject of Section 4, are generated just outside the plasmasphere, near the magnetic equatorial plane. At higher latitude, one finds a plasma sheet (orange). It is a very dynamic region filled with plasma originating both in solar wind and the ionosphere. On the night side, the plasma sheet is elongated along the central part of the Earth magnetotail. This part of the plasma sheet is the subject of Section 3.1. A giant plasma accelerator forms here when equatorial currents supporting the magnetic field topology are disrupted. This happens at the onset of dynamic events that are called substorms, leading to auroral activity near the Earth (source of AKR emissions, subject of Section 2). At even higher latitudes, one finds lobes (yellow in Figure 1). Those are regions that usually are almost void of plasma and they are located on open field lines (one end of the magnetic field lines is anchored in the Earth but another goes into the solar wind). The outer boundary of the lobes and plasma sheet is called the magnetopause (pink thick line), and it separates Earth magnetosphere from the solar wind. Solar wind penetrates into the Earth magnetosphere mainly in the cusp regions placed on the dayside between closed and opened field lines, and at reconnection sites (see Section 3.2). The

P. M. E. Décréau, M. Parrot, and J. -L. Pinçon are with LPCE, CNRS, and Université d'Orléans, Orléans, France; E-mail: pdecreau@cnrs-orleans.fr.

Ph. Louarn is with CESR, CNRS, and Université PaulSabatier, Toulouse, France; E-mail: Philippe.Louarn@cesr.fr.

R. L. Mutel is with the Department of Physics and Astronomy, The University of Iowa, Iowa City, USA; E-mail: robert-mutel@uiowa.edu.

P. Robert is with CETP, CNRS, and Université VSQ, Vélizy, France; E-mail : Patrick.Robert@cetp.ipsl.fr.

A. Vaivads is with the Swedish Institute of Space Physics, Uppsala, Sweden; E-mail: andris@irfu.se

This is one of the invited Commission H Reviews of Radio Science.

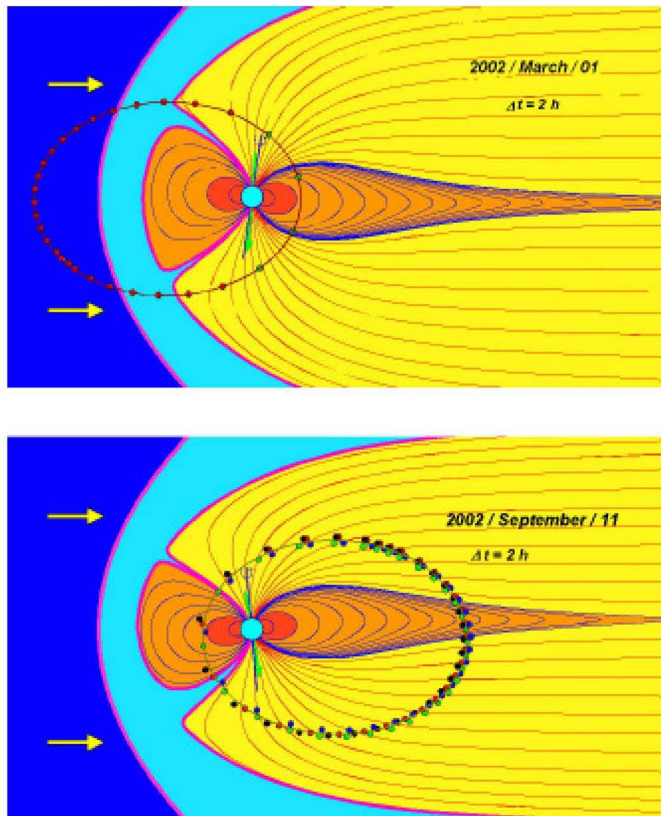


Figure 1. Meridian views of the magnetosphere and Cluster orbit. The magnetic field lines topology corresponds to a static model [2] based on a large data set of instantaneous measurements. It is indicative of the average topology for a given value of the magnetic activity planetary index, K_p , and of the attitude of the Earth magnetic dipole in the GSE frame. Two epochs are chosen, at two different seasons (March 2002, top, and September 2002, bottom). Sketches of the Cluster constellation, at average separations of respectively 100 km (top) and 5000 km (bottom) are drawn along the orbit at time intervals of 2 hours. The topological regions highlighted are: plasmasphere (dark orange), closed field lines outside the plasmasphere (light orange), open field lines (yellow), magnetosheath (turquoise) and solar wind (dark blue). The main boundaries, bow shock (left) and magnetopause, are drawn as thick pink lines.

super sonic solar wind is slowed down at the bow shock (pink thick line on the left), before reaching the magnetopause. In between the bow shock and the magnetopause, the solar wind flows at sub-sonic speed forming the magnetosheath (turquoise), a turbulent region discussed in Section 5.

What could a four spacecraft mission add to this picture?

Since the magnetosphere is constantly in motion, its dynamics is a basic ingredient of its entity. A stationary picture, as detailed as it could be, could not resolve the challenge posed by understanding the physical processes at work [4]. Schematically, in each “cell,” or region, the plasma transport is determined by the coupled effects of the large scale magnetic and electric fields, the size and direction of which are determined by the boundary conditions at the interfaces. Any modeling effort, for instance, would have to be tested again and constrained by realistic, observed, dynamical behaviors at interfaces. Thus the understanding of dynamical behavior of the boundaries can be as important as the understanding of large-scale behavior of different regions. Basic, critical questions related to dynamics of boundaries are still not answered. At the bow shock, for instance, the particles of the solar wind change their motion from global translation into thermal agitation. In the absence of collisions, which processes are at work? In the absence of dissipation, instability mechanisms generating intense fluctuations currently observed at boundaries, are thought to play an important role by coupling adjacent regions. They need to be understood before any realistic picture of the magnetosphere can be drawn.

Observations of dynamical phenomena from a single satellite suffer from a basic limitation: the inability of a single observer to unambiguously distinguish spatial from temporal changes. Only a fleet of four spacecraft can form an observatory able to characterize, in 3D, the motion of a wave front, as of any thin boundary in motion. Actually, the normal direction of interplanetary shocks had been determined by using the ISEE-1, 2, and 3 spacecraft together with either IMP-8 or Prognoz-7 as the fourth [5]. A four spacecraft mission would allow enlarging such isolated case event studies allowed by serendipity to systematic studies. That would be possible not only on morphology and dynamics of boundaries, but also, generally speaking, on all aspects of in-situ characterizing and remote sensing physical processes at play in the magnetosphere. Particularly due to possibility to vary in the spatial lengths to be explored, a four points observatory had to carry the capability to be configured over a range of separation distances.

Once the concept of a four spacecraft fleet accepted and put into reality in the Cluster project, new data analysis techniques and tools had to be developed [6]. When the first Cluster fleet was destroyed in 1996 in the explosion of Ariane 501 maiden flight, the four spacecraft concept was thought so important, remaining a major “step to progress” in the field of magnetospheric physics that, thanks to the conjugated efforts of the main partners involved (nothing would have been possible without a strong involvement of the ESA directorate of science and of national agencies), it came out from ashes. A Cluster II fleet was successfully launched in the summer of 2000.

Since the start of the Cluster mission proper (on February 2001) and the date of this writing, continuous operations have allowed to explore the complete range of MLT apogee positions at several values of the Cluster average separation (in the range 100 to 5000 km). Significant amount of time has been necessary to (i) understand the data of the Cluster scientific payload from the unexplored regions of the magnetosphere, (ii) to understand and use the four spacecraft observatory. In particular, the limitation of observing at only one scale at any step in the mission had to be overcome by selecting relevant events and explaining observations at a deeper level than is necessary with a single satellite. Efforts are still ongoing, but it is already clear that a multipoint fleet brings indeed a novel understanding of a range of magnetospheric phenomena.

1.2 Multi-Point Observations

Five different areas where significant progress has been obtained in the field of wave studies are reported in the paper [two under B]:

- *A, as Auroral Kilometric Radiation (AKR)*, presents an example of remote sensing sources of the high frequency AKR sporadic emissions, by precise measurements of delays in arrival times.
- *B, as Boundary*, presents two examples of in situ spatio-temporal observations. The first one explores the wavy structure of the plasma sheet. The second one concentrates on narrow current layers in the diffusion region linked to magnetic reconnection at magnetopause.
- *C, as Chorus*, illustrates how ray tracing and theoretical modeling could elucidate one of the many observations, some still not explained, where the same wave packet displays different properties as observed from the different spacecraft.
- *D, as Dispersion*, looks into the energy distribution of electro-magnetic fluctuations in various wave modes simultaneously present in the medium. Techniques developed a decade before Cluster launch are shown to work brilliantly.

2. A, as AKR

As seen from deep space, the planet Earth is a powerful radio source, emitting ~ 107 to 108 W, in the form of radio waves with a peak frequency at ~ 250 kHz. Those radiations, emitted well above the dense layers of the ionosphere, at frequencies well below the plasma frequency in those layers, are hidden to ground based observatories. They have been discovered by the Electron -2 satellite [7]. Their spectral properties, observed on OGO 1, were first reported in [8].

In a work of reference, Gurnett [9], analyzing IMP 6 and 8 observations, has established the basic characteristics of this radiation, confirmed by later observations [10 and

references cited therein], in particular its connection with auroral phenomena which led to the terminology “auroral kilometric radiation” [11]. The AKR coherent radiation, displaying multiple facets [12] was intriguing. Several generation mechanisms have been proposed to interpret its properties. Observations on-board the Viking spacecraft [13], well instrumented and crossing regularly AKR sources (at ~ 1 Re altitude), have renewed and sharpened discussions about generation mechanisms. The cyclotron maser instability first proposed by Wu and Lee [14], has been acknowledged as being the most likely candidate [15]. A decade later, observations by the FAST satellite have detailed the AKR source region with order of magnitude higher time and frequency resolution than previous missions [16, 17]. They did not contradict the likeliness of the cyclotron maser instability generation mechanism. Recently, important results about the filamentary nature of AKR sources, and about their dynamics have been derived from Interball 2 observations [18].

The Wideband Data (WBD) instrument on board Cluster [19] collects data at a data rate still higher than on FAST or Interball 2. It was designed to detect very high time ($37 \mu\text{s}$) and frequency (10 Hz) resolution waveform data of plasma and radio waves. In AKR studies, it measures electric field in frequency bands of 10 kHz above one of three frequencies (125, 250 and 500 kHz) chosen by command. It can observe the wave form of AKR emission (translated from high frequency bands) during substantial time intervals, typically a couple of hours, hence complementing information from short wave form captures obtained previously. Those data confirm the bursty character of AKR emissions, already noted in early observations, but at a much higher level of detail.

The remote capture of the AKR signals forbids to rely their individual characteristics to local properties in the source; hence, Cluster cannot directly add to the discussion of generation mechanisms. But, as a remote sentinel, it can instantaneously point to individual AKR burst sources that are sparkling in various parts of an active region. Cluster can recognize that short lived wave packets of few 10 ms total duration, observed by WBD instrument on spacecraft placed at average distances of 5000 km of each other, are coming from the same AKR burst [20, 21].

The recognition method consists in a search of significant peaks in amplitudes of cross-correlation function applied to pairs of signals. Short differential delays in waveform arrival times for each baseline between pairs of spacecraft can be accurately evaluated and used for locating sources as explained below. For baseline connecting spacecraft *i* and *j*, the differential delay is given by:

$$\tau_{ij} = \frac{1}{c} \left[\left| \vec{r} - \vec{s}_j \right| - \left| \vec{r} - \vec{s}_i \right| \right], \quad (1)$$

where \vec{r} is the vector to the AKR source and \vec{s}_{ij} are vectors to spacecraft *i* and *j* respectively (Figure 2a indicates

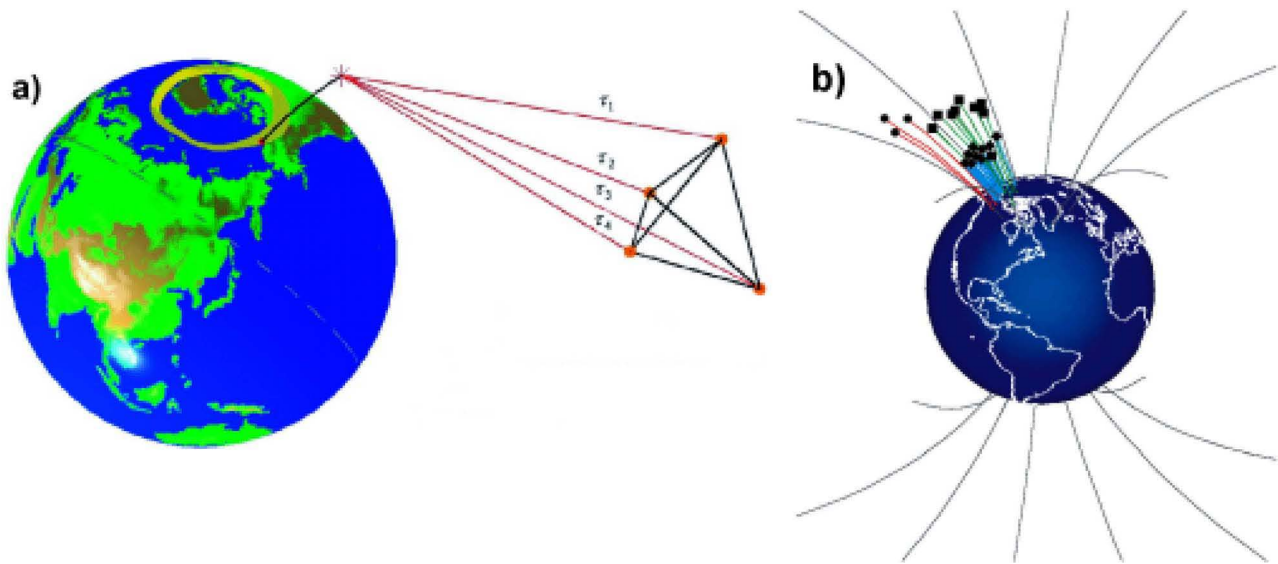


Figure 2. Localization of AKR sources with the VLBI technique (from Mutel et al., [24]): a) delays in AKR bursts arrival times at the four spacecraft allows to locate the source (placed along a magnetic field line, radiating at light speed); b) individual AKR burst location ($0.3 \text{ s} \times 1 \text{ kHz}$ data windows) within a 15 minute time interval centered on 08:22:30 UT, on 9 November 2002. Magnetic field lines connecting burst locations to the Earth's surface are shown as lines coded by AKR burst frequency (125 kHz red, 250 kHz green, 500 kHz blue).

relative positions of source and spacecraft). Solving Equation (1) yields the value of \vec{r} . The delays and spacecraft positions are known at a largely sufficient accuracy: the time stamping applied by NASA's Deep Space Network (DSN) has absolute accuracy of nominally $\pm 0.02 \text{ ms}$, and spacecraft positions provided by the European Space Agency's Operation Centre (ESOC) are measured to $\pm 1 \text{ km}$ or less. Furthermore, there are six baselines, hence six observable delays, therefore the solution for the vector position results in a robust solution algorithm.

In practice, the component along the line of sight to the Cluster constellation centre of mass is less well constrained than the orthogonal coordinates, resulting in perpendicular (\perp along line) of site position uncertainties of respectively 380 – 1400 km (\parallel 26000 – 42000 km) at the AKR burst location. The fact that the source position is defined within an uncertainty volume very elongated along the line of site limits the scientific interest of the result. However, it is possible to reduce the uncertainty volume to a much smaller value by incorporating the well established fact that AKR radiation is emitted at frequencies close to the local gyrofrequency, an approach followed in the past by Huff et al. [22]. Mutel et al. show in [21] that the uncertainty volume is considerably reduced when the allowed source positions are constrained to lie within 3% of the expected geocentric distance consistent with the gyrofrequency of the observed emission. Source position results derived that way can be further analyzed.

The search for correlated AKR bursts is performed by systematic exploration of data windows ($0.3 \text{ s} \times 1 \text{ kHz}$) in all four datasets. Only a small fraction ($\sim 0.2\%$) of the data windows contain well enough isolated AKR burst to result in an unambiguous recognition. Nevertheless, the total

number of AKR burst positions obtained in hours long studies is sufficient to derive systematic statistical properties [21]. The results indicate that the northern AKR sources are located along magnetic field lines threading the statistical auroral oval. This is in good agreement with previous studies on AKR location compared to concurrent auroral images, showing that AKR sources are mapped down to localized auroral features [13, 22]. One should note that in the past, except in a recent case event study with Interball [23], AKR bursts were averaged over significant time intervals (typically a few minutes) hence providing results of intrinsically different nature than WBD measurements (restricted to isolated intense short AKR bursts). Statistics dealing with one or the other type of data could lead to different findings.

Recently published Cluster WBD observations [24], have been able to locate AKR bursts in the three available high frequency bands (each 10 kHz wide) in consecutive 15-minute time intervals over a total time interval of two hours. Figure 2b displays the AKR bursts positions in one of the 15-minute intervals studied. Interestingly, it shows that the AKR emitting volumes related to each emitting frequency (above, respectively, 125, 250 and 500 kHz) are well separated not only in altitudes (to be expected from the constraint of emission at cyclotron resonant altitude) but also in magnetic foot points, a promising step to study direct relationships with auroral images. In addition, distribution of sources over the Southern Hemisphere, which had not yet been investigated, has been obtained. They can be compared to results in Northern hemisphere, opening new perspectives.

As a conclusion, let's remark that temporal relationship of substorms signatures that occur in different regions of space is an important part of substorm research [18, 25, 26].

We believe that the ability to accurately trace AKR bursts, in time, frequency and source position, is an important support to expectations in that field.

3. B, as Boundary

The two illustrations reported in this section deal with the basic problem of resolving spatio-temporal ambiguities within a boundary region. Waves play a different role in both problems. While they constitute the core of the phenomenon under study in the first case, they might be considered as a “marker” of small scale processes in the second case.

3.1 Large Scale Fluctuations in the Plasma Sheet

The Earth magnetic tail is a region of considerable interest in magnetospheric physics, since it is the region of

substorm triggering. The stability of the current sheet (supporting the elongated topology of the tail), as well as its wavy structure, have been observed and theoretically analyzed since decades (see [27, 28] for early works on the subject, and other citations in the introductory section of Louarn et al., [29]). Waves with periods from a fraction of second to a few tens of minutes have been observed, while theoretical analysis of various types of instability indicate that a large variety of perturbations could propagate in current sheets. Multi points observations, which can separate spatial and temporal effects, are crucial toward a correct identification. First case studies with Cluster have displayed unexpected features of the large scale structure and flapping motion of the current sheet [30, 31].

We report here on a series of two papers [29, 33], where multi-spacecraft techniques have been applied to analyze the low frequency fluctuations of the plasma sheet with the objective to determine if they may be interpretable as magneto-hydrodynamic (MHD) eigen modes. To that purpose, a plasma sheet crossing occurring on August 22,

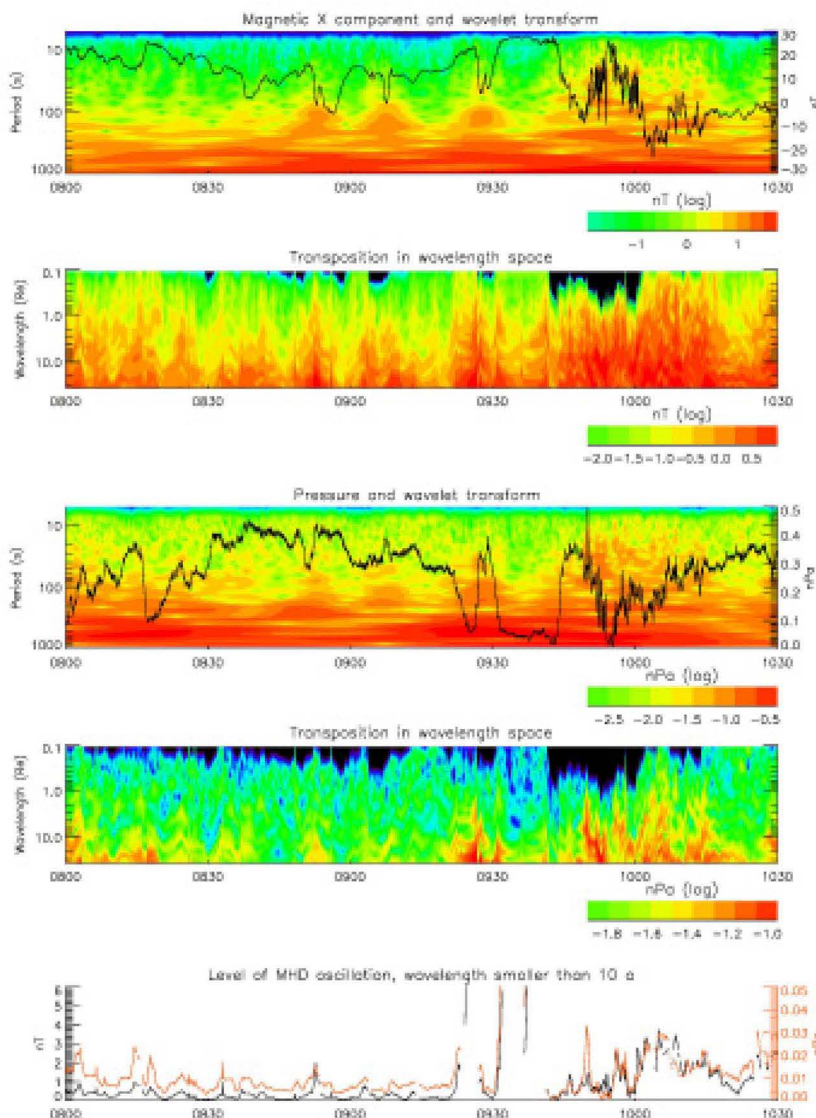


Figure 3. Spatial and temporal scalograms, comparison with the MHD scale of the plasma sheet (from Louarn et al., [29]). Panel (1) and (2): temporal and reconstructed spatial scalograms for the magnetic fluctuations. Panel (3) and (4): same quantities for the pressure fluctuations. Panel (5): integrated amplitude of fluctuations at scales smaller than $10 a$ (a : characteristic thickness of the modeled Harris sheet).

2001 (Figure 3, discussed later), was investigated and the observations were compared with results of a study of the MHD propagation in a one dimensional Harris sheet, which is an exact 1-D solution of both the MHD and the kinetic Vlasov-Maxwell equations. The theory, developed in a preceding work [32], shows that eigen modes have periods scaled by a characteristic time τ roughly equal to the ratio between (1) the thickness of the sheet and (2) the sound speed. Using the Cluster spacecraft, the thickness of the sheet can be determined with accuracy. The characteristic time can then be estimated and compared with the typical periods of the fluctuations that is deduced from a wavelet analysis of the magnetic field and pressure fluctuations (Figure 3).

The August 22, 2001 observations shown in Figure 3 are obtained successively under quiet and disturbed conditions (before and after 0940 UT). During the quiet period, the fluctuations have periods larger than 100-150 s, which corresponds to at least 15 times τ . If they are interpreted as MHD eigenmodes propagating along the sun-earth direction (X axis), they would have wavelength larger than ~ 10 -20 Earth's radius (Re). Such an interpretation is hardly compatible with the actual position of Cluster which is located at ~ 18 Re. However, in relation with a substorm onset (at 0940 UT), fluctuations of shorter period (20 s) are observed. Given the characteristics of the sheet, this corresponds to a few times the characteristic time. These shorter period oscillations, with amplitude as large as 10 nT, likely correspond to the fundamental kink-like eigen mode of the sheet. They would propagate in the earthward/tailward direction with a wavelength of ~ 3 Re. These oscillations have been more quantitatively analyzed (Figure 4). To analyze the spatial-temporal evolution of the sheet, its geometrical parameters are determined from a fit with a Harris sheet [34]. The magnetic field is thus supposed to be written as

$$B_x(z) = B_0 \tanh\left(\frac{z - z_0}{a}\right),$$

where B_0 is the field in the lobe, a the half thickness of the sheet centered at $z - z_0$.

The results are displayed in Figure 4 where the neutral sheet position relatively to Cluster 1 (in blue) and the sheet thickness (in red) are presented in the upper panel. The sheet thickness is ~ 0.4 Re until 0950:30 UT. It then decreases to 0.2 Re from 0951 to 0955:30 UT before increasing gradually again.

Particularly regular oscillations are observed from 0951:30 to 0954, when the sheet is particularly thin, and concern both the position and the thickness which is indicative of the existence of kink and sausage modes. The kink mode corresponds to undulations of the neutral sheet. It is the fundamental mode of the MHD oscillations, it is associated to antisymmetric displacements. The sausage mode corresponds to variation of the thickness of the sheet,

the neutral sheet staying at rest. It is associated to the second harmonic of the MHD oscillations and to symmetric displacements. As seen in panel 2 and 3 where the projection of the normal to the sheet in the plane X/Z and Y/Z is displayed, the observed oscillations also correspond to regular variations of the direction of the normal. They are particularly large (more than 30°) and well-organized in the X/Z plane for the period 0952-0954.

In panel 4, the sheet configuration is reconstructed to get a visual impression of its dynamics. The spacecraft are considered as fix points, their positions along the normal to the sheet being indicated on the plot. Using the sheet position (z_0) and thickness (a), the boundaries of the sheet defined by $z_0 + a$ and $z_0 - a$ are plotted. This plot thus presents the sheet undulations with respect to the spacecraft as a function of time. If these undulations are MHD eigen modes, their phase and group velocities would then be of the order of the sound speed (~ 800 km/s). This plot would then also represent the spatial structure of the sheet.

This presentation of the sheet suggests that the magnetic fluctuations combines both kink and sausage modes. As seen from the blue curve in panel 5, the neutral sheet undulates between Cluster 1 and Cluster 4 spacecraft (labeled SC1 and SC4 in the quoted paper), with a 20-25 s period corresponding to the spectral peak at 0.04 Hz (left plot below panel 5). The sheet thickness fluctuates in remarkable phase with the position which corresponds to the broad peak centered at 0.04 Hz. However, this spectrum also presents a peak at 0.13-0.14 Hz. If they are interpreted in terms of MHD eigen modes, these results suggest that two sausage-like oscillations, at 0.04 and 0.13 Hz, propagate in the sheet. As shown in Fruit et al, [33], a complete model of the linear MHD response of the plasma sheet can be used to theoretically reconstruct the sheet oscillations starting from arbitrary external perturbations. This includes a quantitative prediction of the expected magnetic and pressure fluctuations, of the relative weight of the kink and sausage-like modes as well as the selection of particular resonant frequencies of the sheet. In the present case, it is shown that the kink mode (0.04 Hz) and the high frequency sausage mode are perfectly compatible with the MHD model of Harris sheet oscillations excited by an external perturbation.

This study can be considered as one of the most precise determination of the specific modes of a non-homogeneous plasma structure. It is interesting to note that the MHD model gives a very good interpretation of some of the observed oscillations. However, it is not the lower frequency perturbations that are compatible with the propagation of MHD eigenmodes and clearly, some of the observed oscillations escape the MHD description.

This work illustrates the unprecedented capabilities of Cluster for quantitatively analyzing plasma physics processes with fundamental interrogations concerning the theoretical models that may be used to explain the observations.

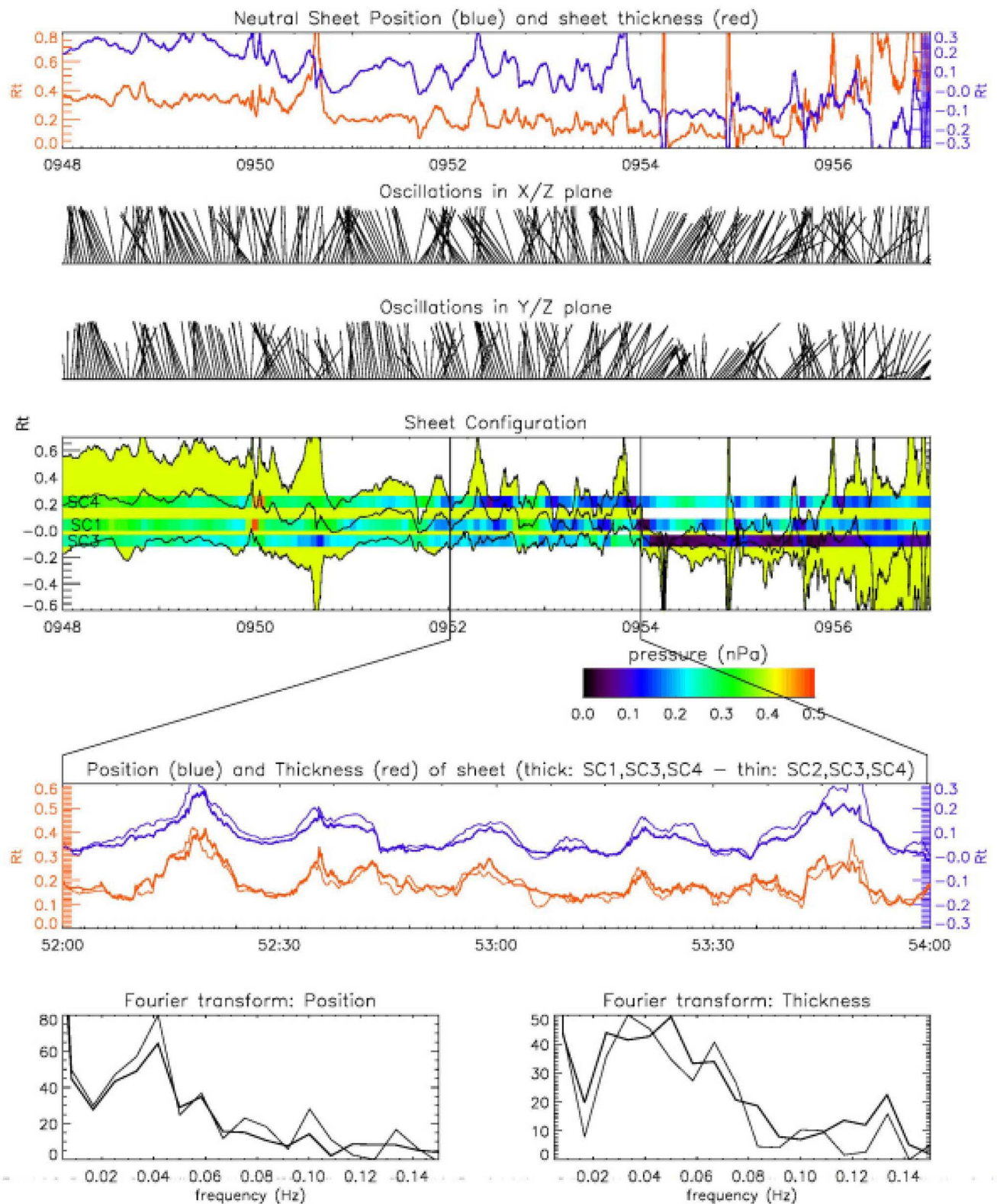


Figure 4. Detailed analysis of the sheet structure (from Fruit et al., [33]). From top panel: (1) neutral sheet position and thickness obtained by a fit with a Harris model; (2) and (3): projections of the normal to the sheet in the X/Z and Y/Z plane; (4) sheet configuration and pressure fluctuations measured by Cluster 1, 3 and 4 spacecraft. (5) and (6): oscillations deduced from STAFF measurements and spectral analysis of thickness and position.

3.2 Waves, as Signatures of Micro-Processes in Small Scale Boundaries

Magnetic reconnection is a major process in astrophysical plasma environments that allows fast conversion of the magnetic field energy of two colliding magnetized plasmas into the kinetic energy of ions and electrons. Better understanding of this phenomenon, key in the dynamics of the magnetosphere, is an important challenge to the Cluster mission. Favorable conditions for the onset of magnetic reconnection are found at locations where narrow current sheets, of the order of the ion inertial length $\lambda_i \approx c/\omega_{pi}$, separate regions in space with nearly opposite directions of the magnetic fields [35, 36]. The reconnection is initiated in small diffusion regions, where the magnetic flux is no longer frozen into the motion of the ions and the electrons.

In a recent study, Vaivads et al. [37] have shown that Cluster could observe for the first time the plasma properties in a diffusion region, without ambiguity in distinguishing spatial and temporal features. On 20 February 2002, around 13–14 UT, the four Cluster spacecraft, separated by an average distance of about 100 km, crossed the magnetopause many times tailward and duskward of the cusp. The study focuses on features on scales in-between the ion and electron scales (particularly traced by waves emissions), at one of the magnetopause crossings. The observations from the Cluster payload are compared with the picture of diffusion region in the neighborhood of the X line as derived from a 2D two fluid simulation. Particularly one is looking for signatures of fast collisionless reconnection [38].

In order to be compared to simulation, Cluster observations have to be placed in the proper reference frame. Top panel of Figure 5 shows results from a 2D two fluid MHD numerical simulation of the diffusion region near the X line [39]. The two directions of reference are respectively the normal N to the discontinuity, and the common direction L of the reconnecting lines. Time delays between the current sheet crossings by different spacecraft give the magnetopause normal direction from observations. This direction is close to the minimum variance direction as obtained by individual spacecraft. The observations of magnetopause are similar on all spacecraft and therefore the diffusion region can indeed be considered as a stable 2D magnetic structure at the scale of Cluster constellation and during the traversal time interval.

Time delays between the current sheet crossings give also the magnetopause velocity, $V_{mp} \approx -120 \text{ km s}^{-1}$, which allows convert temporal variations to spatial variations. Finally, measurements of local plasma parameters on Cluster can be used to normalize distances with respect to the ion inertial length, hence to compare the observation with the simulation results. Density, as well as magnetic field variations compare very satisfactorily (central panel of Figure 5).

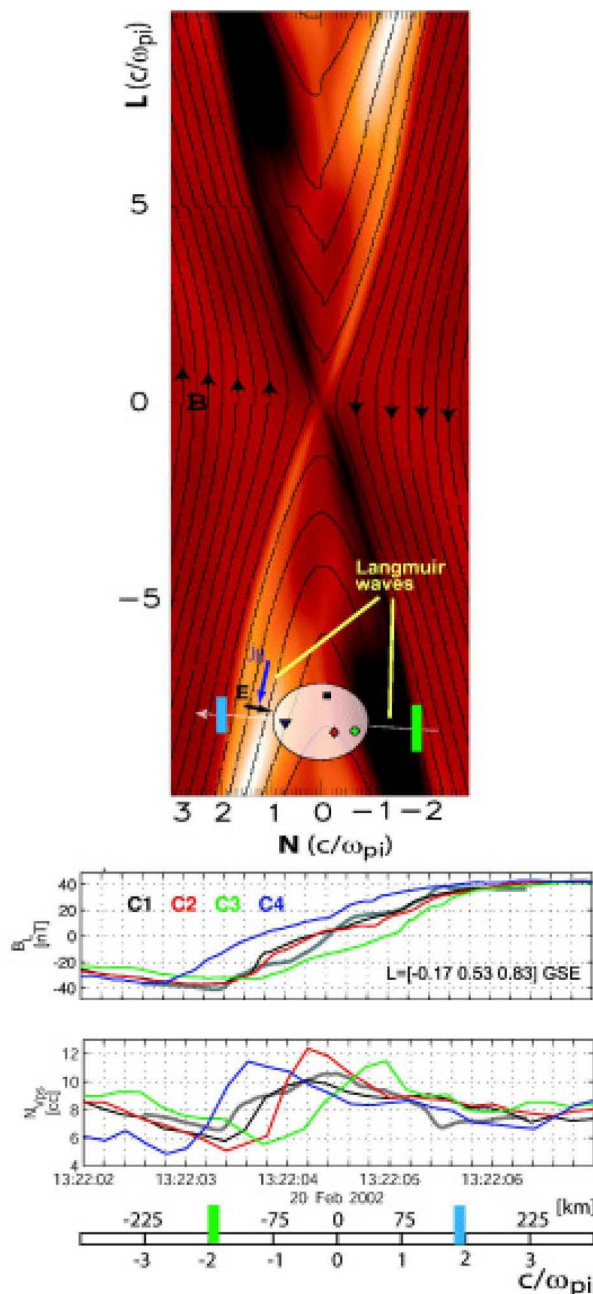


Figure 5. X-line magnetic field configuration observed from a Cluster traversal (reprinted figure with permission from Vaivads et al., *Phys. Rev. Lett.*, **93**, 10, 105001-4, 2004 [37], Copyright (2004) by the American Physical Society). Top 2D structure of the diffusion region from a numerical simulation. The magnetic field lines are shown, and the out-of-plane magnetic field is color coded (white is positive, black negative). The Cluster constellation is projected in the simulation plane. Individual positions are color coded according to a standard code indicated in the panel below, where the four spacecraft are labeled from C1 to C4. Second and third from top observed time variations of the reconnecting (longitudinal) magnetic field component and of plasma density from the satellite potential; simulation results in space are shown with a grey line. Bottom transverse dimension of the structure, expressed in unit of ion inertial length; green and blue rectangles (also drawn at top) mark crossings of the X line branches.

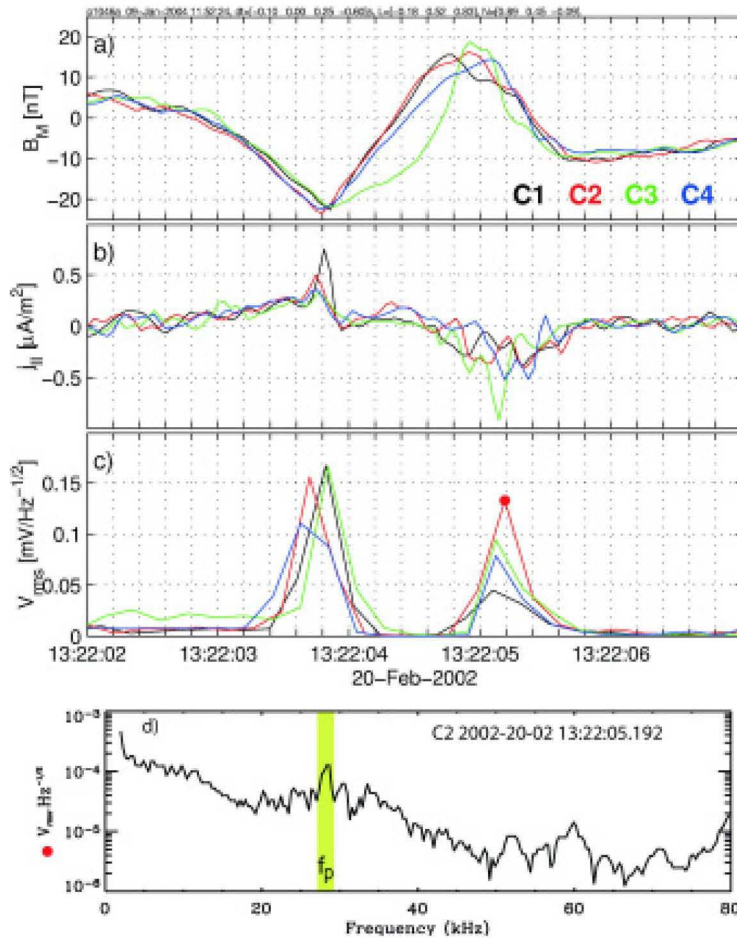


Figure 6. Observations of field-aligned currents and Langmuir/hybrid waves at the separatrices (reprinted figure with permission from Vaivads et al., *Phys. Rev. Lett.*, **93**, 10, 105001-4, 2004 [37], Copyright (2004) by the American Physical Society). The same time interval as in Figure 5; for Cluster 2, 3 and 4 the time series have been shifted -0.09 , -0.3 and $+0.55$ s so that the observations are in the magnetopause frame. (a) out of plane magnetic field component. (b) current parallel to the magnetic field, the direction is away from the X-line. (c) averaged signal amplitude in the frequency range 2 - 80 kHz. (d) wave spectrum from C2 (averaged over 210 ms) at 13:22:05 UT, strong emissions are observed near the plasma frequency, $F_p \sim 28$ kHz.

Cluster observations, shown to mimic the magnetic structure in the N-L plane, can be further examined. Electric field measurements from the EFW instrument [40, 41] (not shown, detailed in [37]), confirm that the model considered is applicable, by indicating a major role of the Hall term in the Generalized Ohm's Law. Figures 6a-6c display three other quantities plotted in the magnetopause frame (time series are shifted adequately). The out-of-plane magnetic field B_M , panel a, shows a bipolar variation with the highest amplitude being $\sim 50\%$ of B_L outside the current sheet. There is no significant offset in B_M , a so called guide field.

According to numerical simulations, the bipolar variation in B_M is an indication of the ion diffusion region in collisionless reconnection and has been used as one of the arguments for ongoing reconnection in previous studies [42], [43]. The third component (not shown), B_N , is non-zero (~ 3 nT) inside the current sheet, which also suggests on-going reconnection. Being $\sim 10\%$ of B_L , it gives a reconnection rate of ~ 0.1 , typical of fast collisionless reconnection [44].

Observations displayed in panels b and c explore the structure at smaller scales. Simulation predicts that a quadrupolar out-of plane magnetic field structure in the diffusion region is caused by current loops that are mainly

perpendicular to the ambient magnetic field in the centre of the current sheet and mainly parallel near the separatrices, directed away from the X-line. The value of parallel currents (panel b) is derived from the variation of magnetic field direction as measured by each of Cluster spacecraft. As predicted by simulations, strong parallel currents occur along the outer edge of the bipolar structure.

Finally, waves at electron scale are taking part in all of this. Examination of a completely independent data set, electric field power integrated over a broad frequency range (including electron plasma frequency) leads to interesting finding: the regions of strong parallel currents are clearly correlated with regions of strong emissions (panel c). Panel d shows the spectra of waves from Cluster 2 in one of the strong emission regions. In addition to broadband spectra there is a spectral peak near the plasma frequency. These waves are probably Langmuir or upper hybrid waves [45].

In summary, Cluster multi-spacecraft measurements allow to unambiguously resolve parallel currents along the separatrices and show that they are correlated with high frequency Langmuir/upper hybrid waves. These waves can be involved in thermalization of electrons, formation of anomalous resistivity, and can be used as a diagnostic tool of reconnection sites.

4. C, as Chorus

Chorus waves are one of the most intense emissions observed in the vicinity of the Earth, just outside the outer boundary of the plasmasphere, called the plasmapause. They are detected near the equatorial plane and they are characterized by a sequence of discrete elements (rising and falling tones) with a time separation between 0.1 and 1 s. They have been extensively studied in the past (see [46] and references cited therein). They are believed to be generated by the injection of substorm electrons [47] through the loss cone instability [48] in the equatorial region. Polar observations, yielding the first Poynting flux measurements of chorus emissions ever performed [49], confirmed that the chorus sources are equatorial. Moreover, they established detailed characteristics of chorus sources [50]. But theoretical efforts are still on-going, aimed at better understanding the exact scenarios and mechanisms of generation. The Cluster fleet has brought new pieces of information which can support those efforts. For the first time, a multi-point mission has been able to find clear correlations between chorus elements observed at several positions in the magnetosphere, thus revealing yet hidden behaviors.

We present below two findings. The first one, published by Parrot et al., [51], is based on observations of the STAFF experiment [52], [53] from Cluster spacecraft placed at an average separation of a few 1000 km: observations for the first time of chorus components reflected at low altitude. The second finding, published by Inan et al. [54], is obtained by WBD instruments placed at separations from about 1000 km to about 100 km: source regions that emit discrete chorus waves are in rapid motion.

4.1 Observation of Reflected Chorus Elements

Detection of a faint chorus emission, after reflection at low altitude, has been possible thanks to an elaborated on-board data processing, part of the STAFF-SA instrument. The processing unit produces 5×5 spectral matrices with 27 frequencies distributed logarithmically between 8 Hz and 4 kHz, at a time resolution which varies between 0.125 and 4 s (4 s for the case event presented). Spectral matrices are further processed on ground by a computer program, PRASSADCO, which adds information from FGM, the magnetometer instrument on Cluster [55, 56]. The program estimates polarization and propagation parameters, including the wave vector and Poynting vector directions.

Figure 7a displays the behavior of banded chorus emission around the magnetic equator. It has been shown [57] that the chorus emission frequency is related to the equatorial cyclotron frequency of the magnetic field line passing through the observing point. Cluster travels on a polar orbit, almost tangent to a magnetic field line near the perigee. The L parameter of the crossed field line is decreasing when Cluster is on its inbound leg (heading toward perigee, from South to North), it is increasing on the outbound leg. The related equatorial cyclotron frequency behaves in the opposite way: increasing, then decreasing, as observed. Observations (shown for Cluster 3) are very similar on the three other spacecraft which, grouped at small distances – a few 100 km – cross the same region about 40 minutes sooner. Figure 7b displays frequency–time spectrograms of the Poynting vector component along the z axis, which is almost normal to the equator. In this

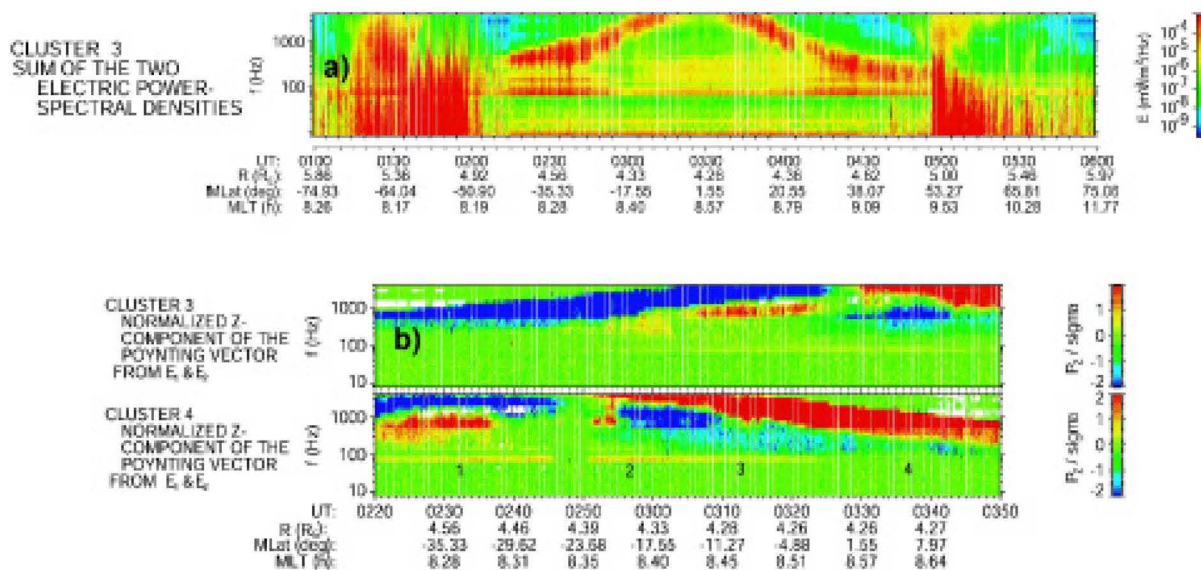


Figure 7. Properties of chorus emissions measured by the STAFF-SA experiment on 29 October 2001 (from Parrot et al., [49]). a) electric power spectral density. Banded emission of chorus type is seen between 100 Hz and 4 kHz, with the maximum frequency being obtained when the Cluster 3 spacecraft (C3) is near the magnetic equator. b) direction of the z-component of the Poynting vector (reliability of the sense of the Poynting vector given by the color-coded scales on the right); compared values from Cluster 3 and Cluster 4 (C4) on a smaller time interval. The geophysical parameters at the bottom are, as on panel a, related to C3.

presentation, Poynting vectors directed along the magnetic field are colored in red, and in blue when they are opposite to the magnetic field. The banded chorus of main intensity shown in Figure 7a is hence propagating away from the equator, as expected for an equatorial source.

In addition to the main banded chorus emission, Figure 7b reveals the presence, close to the equator, of emissions at smaller frequencies with Poynting vectors in the opposite direction (toward the equator). This is the case for instance at ~03:37 UT on Cluster 3 (an event labeled 4 on the panel presenting the Poynting vector for Cluster 4). So that, at the same time and same frequency (~700 Hz), two Cluster spacecraft, both placed in the northern hemisphere, observe potentially the same emission, but propagating in opposite directions. The intensity of the secondary emission is significantly lower than the intensity of the main emission (in a ratio ~0.3%), which explains why it is not apparent in Figure 7a. In order to locate the source of both main and secondary emissions and to critically examine the postulate of a common source for those, Parrot et al. [51] have applied an inverse ray tracing algorithm, using as inputs the polar and azimuthal angles of the wave normal direction (calculated from the PRASSADCO software) during a few minutes time interval. The results of the multiple ray tracing for each satellite and for each polar and azimuthal determinations of the wave normal direction, between 03:32 and 03:42 UT and for a frequency equal to 724 Hz, are shown in Figure 8. Stopped when the ray reaches the equator, they locate the source in the same area, hence supporting the postulate that Cluster 3 observes chorus elements having undergone a reflection at low altitudes (when the frequency of the wave approaches the local LHR frequency). The intensity ratio between the direct and the reflected waves corresponds roughly to estimations [58], forming another supporting piece of evidence. Lastly, the wave form of emissions identified by the STAFF instrument as “reflected chorus” has been

measured by the WBD instrument [59]. Their frequency/time behavior confirms the postulate that Cluster 3 observed the same emission than Cluster 4, the former coming directly from the equator and the latter after reflection at low altitude.

4.2 Remote Sensing Moving Chorus Sources

Observing chorus elements of higher central frequencies (above STAFF frequency range) with the WBD instrument, Gurnett et al., [20], noted puzzling differences in detailed observations of the same chorus elements: frequency differences Δf of order 1 kHz, and time differences Δt of order 0.1 s. The differences in frequency, as well as the different times of arrival at the different spacecraft, could be explained by Inan et al. [54]. They invoked rapid motion of the compact source regions of chorus, traveling at speeds comparable to the parallel resonance velocity of counter-streaming electrons moving along the Earth’s magnetic field lines (the underlying mechanism for generation of ELF/VLF chorus is believed to be the cyclotron resonance interaction). Waves emanating from a compact source can reach two different observers, as Cluster 1 and Cluster 2 spacecraft, only by propagating at two different wave normal angles, and are thus observed at two different “apparent” frequencies. The authors, analyzing three event cases, determined that the sources were moving at speeds of $20,000 \text{ khs}^{-1}$ to $25,000 \text{ khs}^{-1}$ toward the observer.

Only a multiple spacecraft mission, equipped with identical instrumentation of high performances, could derive such an estimation, opening new capabilities for studying the dynamic character of chorus emissions, reported in other studies based on Cluster data [60, 61, and 62].

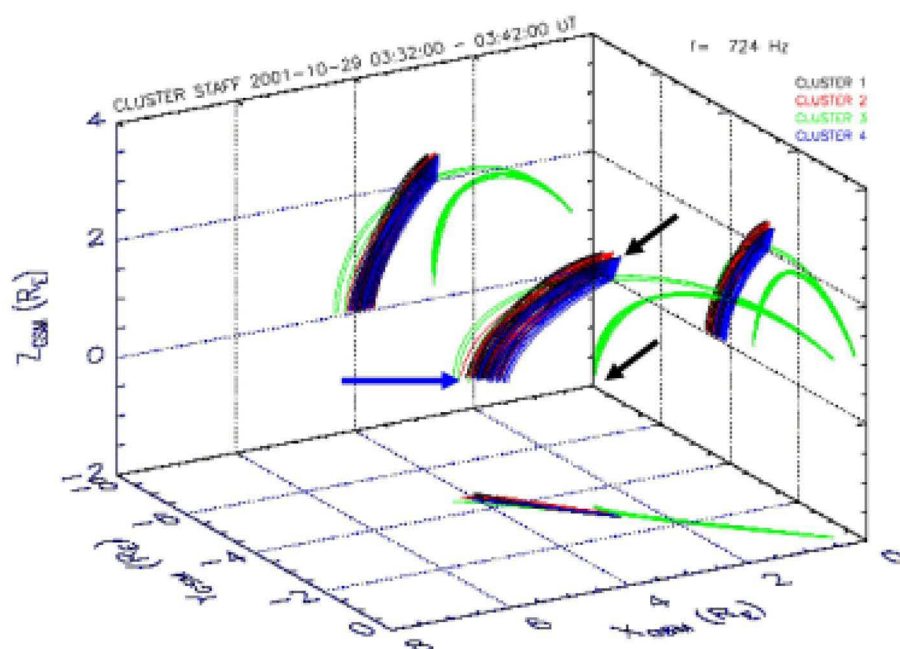


Figure 8. Plots of the ray traces in 3-D and their corresponding projections on the three planes for the time interval 03:32 – 03:42 UT and for a frequency equal to 724 Hz (from Parrot et al., [49]). A blue arrow points to the source area. Black arrows point to Cluster positions when they observe the event.

5. D, as Dispersion

In this section we report what is perhaps the most spectacular outcome of a four spacecraft observatory, in term of wave studies. Locally observed magnetic and electric fluctuations are analyzed via a true 3D tool which identifies \mathbf{k} wave vectors where the energy is propagating. The analysis can be done systematically over a range of frequencies. Wave mode identification is obtained by comparing the identified \mathbf{k} values with theoretical dispersion relations adjusted to the local characteristics of the medium. Applying this approach to turbulent like ULF magnetic fluctuations observed in the magnetosheath, it has been demonstrated that the energy does indeed propagate on several plane waves (i.e., with several wave vectors) with comparable energies, revealing a complex physics. No set of assumptions associated to mono-satellite data, however elaborated, could have yielded such a result.

5.1 k -Filtering – Wave Telescope Technique

k -filtering [63], also called the wave telescope technique when restricted to magnetic field fluctuations, identifies 3D-structures in the wave fields. Developed in the context of space plasma physics by Pinçon and Lefeuvre [64], it was applied successfully to Cluster data from FGM instrument [65] and to data from the STAFF-SC and the EFW instruments [66, 67]. Given a measured wave field $\mathbf{B}(t, \mathbf{r}_\alpha)$ at the position \mathbf{r}_α ($\alpha=1, 2, \dots$), k -filtering estimates the 4D-energy distribution function $P(\omega, \mathbf{k})$ related to the wave field \mathbf{B} , assuming that (i) the measured waveform is described as a superposition of plane waves, (ii) fields are translation invariant on distances and stationary on time intervals larger than respectively the studied wavelengths and wave periods, and (iii) the wave field does not contain waves of length shorter than the inter-spacecraft separation. Correlation matrices $\mathbf{M}(\omega, \mathbf{r}_{\alpha\beta})$ are calculated

by correlating (over a chosen time interval) measured wave fields (expressed in the frequency domain) at positions \mathbf{r}_α and \mathbf{r}_β . From all correlation matrices constructed from the Cluster quartet, one forms the (12×12) $\mathbf{M}(\omega)$ matrix, which, transformed according to a geometrical matrix $\mathbf{H}(\mathbf{k})$ depending on the positions on the four satellites, yields the distribution function $P(\omega, \mathbf{k})$. For given frequency $\omega(\mathbf{k})$, k -filtering allows identifying several waves (i.e. several wave vectors \mathbf{k}) carrying different power levels.

5.2 Case Study of High Beta Plasma Parameters

Data used for this case study were obtained around 05:34:00 UT on 18 February 2002. The spacecraft were in the magnetosheath near the magnetopause, separated by about 100 km. The Cluster configuration associated with this data set was checked to correspond to a real 3D configuration (elongation and planarity parameters small enough [68]). The magnetosheath parameters are derived from the Cluster instruments. Averaged magnetic field is measured to be about (5.4, -20.2, 1.2) nT in GSE frame, plasma density from the resonant sounder [69] is about 36 cm^{-3} . Parallel and perpendicular ion temperatures are measured by the CIS instrument [70] to be about 140 eV and 170 eV respectively, and the electron temperature (not available) is known to be typically of the order of 40 eV.

Key parameters are thus obtained: Alfvén velocity $V_a \approx 78 \text{ km s}^{-1}$; ion gyro-frequency $f_{ci} \approx 0.33 \text{ Hz}$; ion Larmor radius, $\rho \approx 79 \text{ km}$, and ion anisotropy parameter $A_i \gg 0.22$. The beta parameters, much larger than unity, are mainly due to ions, with parallel and perpendicular estimations respectively equal to 4.5 and 5.4; the electron pressure is likely to have a negligible role in the wave physics in this case event.

A time interval of 164 s is selected for the analysis. Magnetic data from the STAFF instrument are filtered

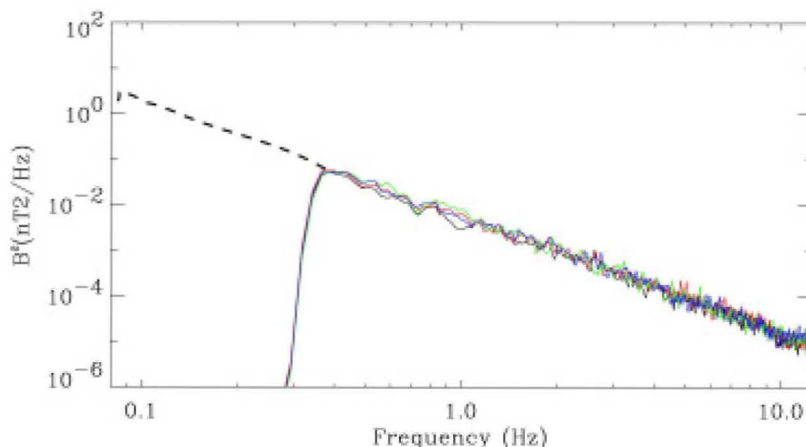


Figure 9. Power spectrum of the ULF magnetic fluctuations (from Sahraoui et al., [64]). The event studied is a 164 s time interval, starting at 05:34:01.15 UT on 18 February 2002, wave form filtered at the cut off frequency 0.35 Hz. This spectrum is close to a power-law $f^{-\alpha}$, with $\alpha = 2.2$. The colored lines represent data from Cluster 1 (black), 2 (red), 3 (green), and 4 (blue).

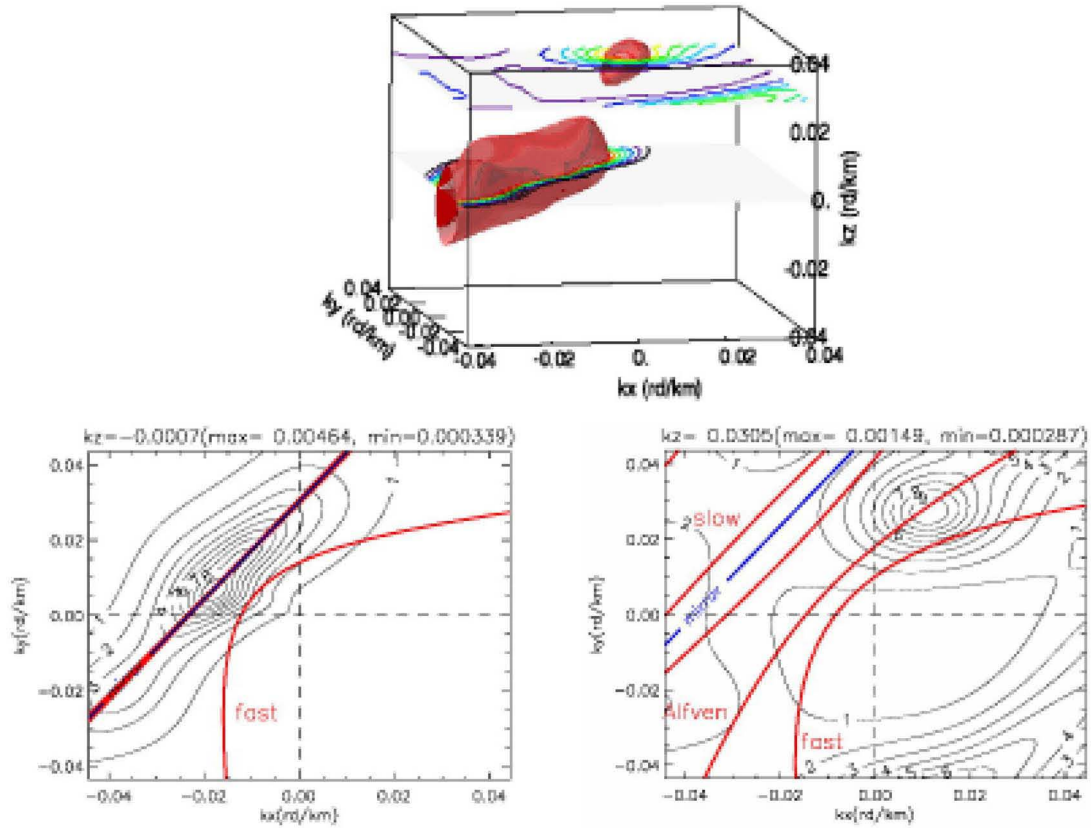


Figure 10. A presentation of the magnetic field distribution, noted MFED, associated with frequency 0.61 Hz in the (k_x, k_y, k_z) domain. Top: 3D view (see text). Bottom (from Walker et al., [65]): superposition of the experimental magnetic energy (thin black lines) with the theoretical dispersion relations of the LF modes (colored thick lines) in the MFA frame for the frequency 0.61 Hz. The blue line is the Doppler shift $\omega = k \cdot v$. Two main peaks are identified: a mirror mode (left panel) and an Alfvén wave (right panel) having a frequency in the plasma frame close to the second gyroharmonic $F_{\text{plasma}} = 0.71 \text{ Hz} \sim 2 F_{ci}$.

using a high-pass filter with a cut-off frequency of 0.35 Hz, in order to filter out any possible spurious signal linked to the spin frequency (0.25 Hz). The power spectrum of the filtered magnetic fluctuations, shown in Figure 9, displays a smooth intensity decay with frequency, identical on all four spacecraft, with a slope parameter consistent with a turbulent cascade of energy from large to small scale [66].

When analyzed by the k -filtering tool, the same data indicate a clear organization. The power of the wave at a selected frequency, f , is distributed over two main volumes in \mathbf{k} space. Results are displayed in Figure 10 (at $f = 0.61$ Hz) using the Magnetic Field Aligned (MFA) referential, which is defined as follows: z axis is along the mean magnetic field $B_0 = B_0 \mathbf{z}$, the x axis is perpendicular to the z axis, in the plane containing the Sun-satellite line and the z axis, and is directed towards the Sun, and the y axis completes the right-handed coordinate system. In the upper panel, the 3D view of the magnetic wave field energy distribution in \mathbf{k} space, noted MFED, is obtained by displaying the iso-surface in energy per unit of \mathbf{k} volume, corresponding to 33% of the maximum value.

As can be seen, the two iso-surfaces, linked to the two main volumes in \mathbf{k} space, are well separated. They are placed near two (k_x, k_y) planes with $k_z = -0.0007 \text{ rd km}^{-1}$ and $k_z = 0.0305 \text{ rd km}^{-1}$ respectively. Each (k_x, k_y) plane is restricted to the validity domain defined by $k_x, k_y \in [-0.04; 0.04] \text{ rd km}^{-1}$. The validity domain in \mathbf{k} space is determined from the separations between the Cluster satellites: all the existing wavelengths have to be larger than the satellites separations, which are of the order of 100 km in the present case. In the lower panels of Figure 10 (from [67]), the wave field energy distribution is displayed in the two (k_x, k_y) planes quoted above, linked to the two distinct volumes of significant MFED maxima. Lines of iso-energy are marked by level values associated in each case to the max and min values indicated on the figures.

In order to identify the wave mode associated with each MFED volume, Sahraoui et al. [66] calculated the linear dispersion relations of the low frequency modes: mirror, Alfvén, fast and slow magnetosonic modes. Results are plotted in the two (k_x, k_y) planes determined from

observations. Because theoretical values are naturally obtained in the plasma frame, one has to take into account the Doppler effect. The relative velocity between the plasma and the Cluster constellation is provided by the CIS ion analyzer. The Doppler is then easily estimated for each k value, and used to obtain the theoretical dispersion results plotted in red. The mirror mode is considered as a non-propagating mode ($\omega = 0$) in the plasma frame.

The comparison of theoretical dispersion relation with observations in Figure 10 clearly identifies the two superposed modes of propagation at 0.61 Hz as modes obeying the linear dispersion relation of ULF wave modes. The mirror mode, Doppler shifted to nonzero frequencies in the MFA frame, is confirmed to be the dominant mode in the high b plasma analyzed in this case. An Alfvén wave mode (bottom right panel), about three times lower in intensity, is also present. Similar analysis at other frequencies indicates that the observed magnetic field energy is distributed over several eigen modes close to the theoretical ULF mirror, Alfvén, and slow mode. This result suggests that weak non linear interaction between low frequency modes might counteract the effects of linear kinetic damping. A further analysis of the event [72] (using complementary data, from the magnetometer FGM instrument) confirms the presence of non linear processes. The study indicates that the magnetic energy seems to be injected over the low frequency (FGM band) part of the observed spectrum, at a spatial scale that is in very good agreement with the predicted maximum growth rate of the mirror instability. The validity of a model of weak turbulence is foreseen to be explored in the future [73].

6. Concluding Remarks

This short panorama of findings is a partial and incomplete view. It leads however to a few reflections.

1. What the mission designers “had always wanted to do,” i.e. 3D characterization, has been accomplished, as shown by the illustrations presented at both ends of the panorama (the AKR and Dispersion sections). In terms of remote sensing, the WBD instrument, served by the DSN network, had the unique opportunity to try VLBI on terrestrial radiation, hence deriving a new category of results. In terms of local wave characterization, the k filtering method has proven to be applicable in the ULF domain, not only in the magnetosheath region, case of the chosen illustration, but for instance in the foreshock [74]. Turbulent plasma regimes which could be studied only from statistics that mixed spatial and temporal variations, are now understood as natural properties of the flowing plasma, opening a brand new field of investigation. It is worth noting that the k filtering method is not the only way to obtain a 3D characterization of the waves. Other methods have been elaborated and successfully applied to Cluster data [67, 75, 76, 77, 78]. They can bring complementary information to the k

filtering method, the most powerful in sorting out several co-existing waves, but requiring a reasonably stationary signal. Such a requirement is not necessary, for instance, with the instantaneous local wave analysis [76]. Cluster, hence, provides a good opportunity for further tests on various wave analysis tools.

2. Boundaries, those key regions “where the action is” have been explored in a way as to disentangle time and space variations. Boundary studies rely heavily on independent determinations of the local orientation of the boundary, which provide the adequate frame of study. One should underline the essential role of large-scale magnetic field data and of a 3D (four points) spacecraft fleet to this end. Elaborated tools continue to be developed to support boundary studies, for instance toward a reconstruction of a 2D spatial topology from multi-point temporal variations [79].

The illustrations presented in this review are only a sample of the many findings obtained by Cluster exploring boundaries and their wavy structures. Concerning large and mesoscale structures, one can cite for instance characterization of SLAMS (Short Large Amplitude Magnetic Structures) near the bow shock [80], of bow shock global oscillations [81], of Kelvin-Helmholtz vortices at the magnetopause [82], and of current sheet oscillations [83, 84]. Structures at smaller scales in the vicinity of the bow shock are reported in [85] and [86]. Magnetic turbulence analysis in the current sheet is reported in [87]. Lastly, the multi-point Cluster analysis allow to better characterize ELF and VLF waves present for instance near the electron foreshock boundary [88, 89], in the polar cusp [90], or in the vicinity of the plasmopause boundary [91, 92].

As expected, Cluster brought also “good surprises,” as demonstrated by chorus studies (Section 4). Indeed, it was not granted that the instrument’s sensitivity would be good enough to detect a reflected chorus radiation, nor that the direct radiation would be in view of another Cluster point, right in time for confirmation of the reflection hypothesis. Likewise, that small frequency and time shifts of the same chorus element as observed from different view points could be measured, and thus lead to a model of chorus drifts and an estimation of their velocity. There are many more findings to come in this category.

1. Other types of Cluster findings in the field of wave studies are not covered by this rapid overview. Important ones are related to very small scale processes (like solitary waves reported in [93, 94]), others to multiple scale studies, in particular in conjunction with ground observations, others to wave particle interactions (see for instance [95]). We can recommend the interested reader to have a look at the Cluster publication list [96].
2. Expectations for the future are that many findings are still to be discovered, some likely by “work in progress,” in particular statistics on various phenomena. After four

years of operations as a tetrahedron of regular shape over large parts of the orbit (surveying phenomena with some coherence over a volume of space), Cluster will, in the near future, be configured to larger baselines, which among other capabilities will allow better remote sensing of wave sources like continuum radiations, where first multi-point Cluster results are promising [97, 98].

Finally, Cluster exploration of waves, yielding either confirmations of expected behaviors or discovery of non expected behaviors, will guide global simulations and theoretical studies, toward a better understanding of the mysteries of the magnetosphere equilibrium and dynamics – among others the mechanism of substorm triggering, of turbulence and dissipation in large scale boundaries, of energy and momentum transfers at thin boundaries; all of general interest to the fields of astrophysics and plasma physics.

7. Acknowledgements

This paper is dedicated to the memory of Les Woolliscroft, the principal investigator of DWP [99], one of the WEC (Wave Experiment Consortium) instruments on Cluster, until his ultimate demise. Les, as the head of the WEC group, played a determining role in shaping the scientific payload, which is working beautifully on all four Cluster spacecraft. Most of the material included in the paper is directly borrowed from published papers, whose authors should take the credit for the reported findings. Parts of the introductory section are borrowed from publications of A. Roux and G. Pashmann, who played a leading role in the Cluster mission concept. Finally, we are grateful to all mission teams for their dedication in managing the heavy load of operating the first 3D magnetospheric observatory. Our friendly thanks in particular to J. Pickett, D. A. Gurnett, M. André, G. Gustafsson, A. Erikson, P.-A. Lindqvist, N. Cornilleau-Wehrlin, M. Maksimovic, P. Canu, H. Alleyne, K. Yearby, A. Balogh and E. Lucek, leading members of the WEC and FGM teams.

8. References

- G. Pashmann, "The Fourfold Way Through the Magnetosphere: The Cluster Mission," published by the Association Pro ISSI, *SPATIUM*, **9**, 2002.
- N. A. Tsyganenko, A. V. Usmanov, V. O. Papitashvili, V. A. Popov, "Software for Computations of the Geomagnetic Field and Related Coordinate Systems," Academy of Sciences of USSR, Soviet Geophysical Committee, Special Report, 58 p., Moscow, 1987.
- C. T. Russell, "A Brief History of Solar-Terrestrial Physics," in C. T. Russell and M. G. Kivelson (eds.), *Introduction to Space Physics*, Cambridge, UK, Cambridge University Press, 1995, pp. 1–26.
- A. Roux, "La mission spatiale Cluster," *Nouvelle revue d'aéronautique et d'astronautique*, **3**, 37, 1996.
- C. T. Russell, J. T. Gosling, R. D. Zwickl, and E. J. Smith, "Multiple Spacecraft Observations of Interplanetary Shocks ISEE Three-Dimensional Plasma Measurements," *J. Geophys. Res.*, **88**, 9941, 1983.
- G. Pashmann and P. Daly (eds.), *Analysis Methods for Multi-Spacecraft Data*, Bern: ISSI, 1998.
- E. A. Benediktov, G. G. Getmantsev, Yu A. Sazonov, and A. F. Tarasov, "Preliminary Results of Measurements of the Intensity of Distributed Extraterrestrial Radio Frequency Emission at 725 and 1525 kHz by the Satellite Electron-2," *Kosm. Issled.*, **3**, 614, 1965. (*Cosmic Res.*, Engl. Transl., **3**, 492, 1968).
- N. Dunkel, B. Ficklin, L. Rorden, and R. A. Helliwell, "Low Frequency Noise Observed in the Distant Magnetosphere with OGO 1," *J. Geophys. Res.*, **75**, 1,854, 1970.
- D. A. Gurnett, "The Earth as a Radio Source: Terrestrial Kilometric Radiation," *J. Geophys. Res.*, **79**, 4227, 1974.
- R. F. Benson, "Auroral Kilometric Radiation: Waves Modes, Harmonics, and Source Region Electron Density Structures," *J. Geophys. Res.*, **90**, 2753, 1985.
- W. S. Kurth, M. M. Baumbach, and D. A. Gurnett, "Direction-Finding Measurements of Auroral Kilometric Radiation," *J. Geophys. Res.*, **80**, 2764, 1975.
- M. M. Mellott, W. Calvert, R. L. Huff, and D. A. Gurnett, "DE 1 Observations of Ordinary Mode and Extraordinary Mode Auroral Kilometric Radiation," *Geophys. Res. Lett.*, **11**, 1188, 1984.
- A. Bahnsen, B. M. Pedersen, M. Jespersen, E. Ungstrup, L. Eliasson, J. S. Murphree, R. D. Elphinstone, L. Blomberg, G. Holmgren, and L. J. Zanetti, "Viking Observations at the Source Region of Auroral Kilometric Radiation," *J. Geophys. Res.*, **94**, 6643, 1989.
- C. S. Wu, and L. C. Lee, "A Theory of the Terrestrial Kilometric Radiation," *Astrophys. J.*, **230**, 621, 1979.
- P. Louarn, A. Roux, H. de Féraudy, D. Le Quéau, and M. André, "Trapped Electrons as a Free Energy Source for the Auroral Kilometric Radiation," *J. Geophys. Res.*, **95**, 5983, 1990.
- G. T. Delory, R. E. Ergun, C. W. Carlson, L. Muschietti, C. C. Chaston, W. Peria, J. P. MacFadden, and R. Strangeway, "FAST Observations of Electron Distributions with AKR Source Regions," *Geophys. Res. Lett.*, **25**, 2069.
- R. E. Ergun, C. W. Carlson, J. P. McFadden, F. S. Mozer, G. T. Delory, W. Peria, C. C. Chaston, M. Temerin, R. Elphic, R. Strangeway, R. Pfaff, C. A. Cattell, D. Klumpp, E. Shelly, W. Peterson, E. Moebius, and L. Kistler, "FAST Satellite Wave Observations in the AKR Source Regions," *Geophys. Res. Lett.*, **25**, 2061, 1998.
- J. Hanasz, H. de Féraudy, R. Schreiber, G. Parks, M. Brittnacher, M. M. Mogilevsky, and T. V. Romantsova, "Wideband Bursts of Auroral Kilometric Radiation and their Association with UV Auroral Bulges," *J. Geophys. Res.*, **106**, 3859, 2001.
- D. A. Gurnett, R. L. Huff, and D. L. Kircher, "The Wide-Band Plasma Wave Investigation," *Space Science Reviews*, **79**, 195, 1997.
- D. A. Gurnett, R. L. Huff, J. S. Pickett, A. M. Persoon, R. L. Mutel, I. W. Christopher, C. A. Kletzing, U. S. Inan, W. M. Martin, J.-P. Bougeret, H. St. Alleyne, and K. H. Yearby, "First Results from the Cluster Wideband Plasma Wave Investigation," *Ann. Geophys.*, **19**, 1259, 2001.
- R. L. Mutel, D. A. Gurnett, I. W. Christopher, J. S. Pickett, and M. Schlax, "Locations of Auroral Kilometric Radio Bursts Inferred from Multispacecraft Wideband Cluster VLBI Observations. 1. Description of Technique and Initial Results," *J. Geophys. Res.*, **108**, 1398, doi:10.1029/2003JA010011, 2003.
- R. L. Huff, J. D. Calvert, L. A. Frank, and D. A. Gurnett, "Mapping of Auroral Kilometric Radiation Sources to the Aurora," *J. Geophys. Res.*, **93**, 11,445, 1988.
- R. Schreiber, O. Santolik, M. Parrot, F. Lefeuvre, J. Janasz, M. Brittnacher, and G. Parks, "Auroral Kilometric Radiation

- Source Characteristics Using Ray Tracing Techniques,” *J. Geophys. Res.*, **107**, 1381, doi:10.1029/2001JA009061, 2002.
24. R. L. Mutel, D. A. Gurnett, and I. W. Christopher, “Spatial and Temporal Properties of AKR Burst Emission Derived from Cluster WBD VLBI Studies,” *Ann. Geophys.*, **22**, 2625, 2004.
 25. K. Liou, P. T. Newell, C.-I. Meng, A. T. Y. Lui, M. Brittnacher, and G. Parks, “Dayside Auroral Activity as a Possible Precursor of Substorm Onsets: A Survey Using Polar Ultraviolet Imagery,” *J. Geophys. Res.*, **102**, 19835, 1997.
 26. K. Liou, C.-I. Meng, A. T. Y. Lui, P. T. Newell, and R. R. Anderson, “Auroral Kilometric Radiation at Substorm Onset,” *J. Geophys. Res.*, **105**, 25535, doi 10.1029/2000JA000038, 2000.
 27. V. L. Patel, “Magnetospheric Tail as Hydromagnetic Wave Guide,” *Phys. Lett.*, **26A**, 596, 1968.
 28. G. L. Siscoe, “Resonant Compressional Waves in the Geomagnetic Tail,” *J. Geophys. Res.*, **74**, 6482, 1969.
 29. P. Louarn, G. Fruit, E. Budnik, J. -A. Sauvaud, C. Jacquy, D. Le Quéau, H. Rème, E. Lucek, and A. Balogh, “On the Propagation of Low-Frequency Fluctuations in the Plasma Sheet: 1. Cluster Observations and Magnetohydrodynamic Analysis,” *J. Geophys. Res.*, **109**, A03216, doi: 10.1029/2003JA010228, 2004.
 30. T. L. Zhang, W. Baumjohann, R. Nakamura, A. Balogh, and K. -H. Glassmeier, “A Wavy Twisted Neutral Sheet Observed by Cluster,” *Geophys. Res. Lett.*, **29**, 19, 1899, doi: 10.1029/2002GL015544, 2002.
 31. V. Sergeev, A. Runov, W. Baumjohann, R. Nakamura, T. L. Zhang, M. Volwerk, A. Balogh, H. Rème, J. -A. Sauvaud, M. André, and B. Klecker, “Current Sheet Flapping Motion and Structure Observed by Cluster,” *Geophys. Res. Lett.*, **30**, 6, doi: 10.1029/2002GL016500, 2003.
 32. G. Fruit, P. Louarn, A. Tur, and D. Le Quéau, “On the Propagation of Magnetohydrodynamic Perturbations in a Harris-Type Current Sheet, 1. Propagation on Discrete Modes and Signal Reconstruction,” *J. Geophys. Res.*, **107**, A11, 1411, doi: 10.1029/2001JA009212, 2002.
 33. G. Fruit, P. Louarn, E. Budnik, J. -A. Sauvaud, C. Jacquy, D. Le Quéau, H. Rème, E. Lucek, A. Balogh, and N. Cornilleau-Wehrin, “On the Propagation of Low-Frequency Fluctuations in the Plasma Sheet: 2. Characterization of the MHD Eigenmodes and Physical Implications,” *J. Geophys. Res.*, **109**, A03217, doi: 10.1029/2003JA010228, 2004.
 34. E. G. Harris, “On a Plasma Sheath Separating Regions of Oppositely Directed Magnetic Field,” *Nuovo Cimento*, **23**, 115, 1962.
 35. J. Birn, J. F. Drake, M. A. Shay, B. N. Rogers, R. E. Denton, M. Hesse, M. Kuznetova, Z. W. Ma, A. Bhattacharjee, A. Otto, and P. L. Pritchett, “Geospace Environmental Modeling (GEM) Magnetic Reconnection Challenge,” *J. Geophys. Res.*, **106**, 3715, 2001.
 36. M. Schöler, I. Sidorenko, C. H. Jaroschek, R. A. Treumann, and A. Zeiler, “Onset of Collisionless Magnetic Reconnection in Thin Current Sheets: Three-Dimensional Particle Simulations,” *Physics of Plasmas*, **10**, 9, 3521, 2003.
 37. A. Vaivads, Y. Khotyaintsev, M. André, A. Retino, S. C. Buchert, B. N. Rogers, P. Décréau, G. Pashmann, and T. Phan, “Structure of the Magnetic Reconnection Diffusion Region from Four-Spacecraft Observations,” *Phys. Rev. Lett.*, **93**, doi: 10.1103/PhysRevLett.93.105001, 2004.
 38. M. E. Mandt, R. E. Denton, and J. F. Drake, “Transition to Whistler Mediated Magnetic Reconnection,” *Geophys. Res. Lett.*, **21**, 73, 1994.
 39. B. N. Rogers, R. E. Denton, J. F. Drake, and M. A. Shay, “Role of Dispersive Waves in Collisionless Magnetic Reconnection,” *Phys. Rev. Lett.*, **87**, 19, 195004, 2001.
 40. G. Gustafsson, R. Boström, B. Holback, G. Holmgren, A. Lundgren, K. Stasiewicz, L. Åhlén, F. S. Mozer, D. Pankow, P. Harvey, P. Berg, R. Ulrich, A. Pedersen, R. Schmidt, A. Butler, A. W. C. Fransen, D. Klinge, M. Thomsen, C. -G. Fälthammar, P. -A. Lindqvist, S. Christenson, J. Holtet, B. Lybekk, T. A. Sten, P. Tanskanen, K. Lappalainen, and J. Wygant, “The Electric Field and Wave Experiment for the Cluster Mission,” *Space Sci. Rev.*, **79**, 1997, pp. 137–156.
 41. G. Gustafsson, M. André, T. Carozzi, A. I. Eriksson, C. -G. Fälthammar, R. Grard, G. Holmgren, J. A. Holtet, N. Ivchenko, T. Karlsson, Y. Khotyaintsev, S. Klimov, H. Laakso, P. -A. Lindqvist, B. Lybekk, G. Marklund, F. Mozer, K. Mursula, A. Pedersen, B. Popielawska, S. Savin, K. Stasiewicz, P. Tanskanen, A. Vaivads, and J. -E. Wahlund, “First Results of Electric Field and Density Observations by Cluster EFW Based on Initial Months of Operation,” *Ann. Geophys.*, **19**, 1219, 2001.
 42. T. Nagai, I. Shinohara, M. Fujimoto, M. Hoshino, Y. Saito, S. Machida, and T. Mukai, “Geotail Observations of the Hall Current System: Evidence of Magnetic Reconnection in the Magnetotail,” *J. Geophys. Res.*, **106**, 25929, 2001.
 43. A. Runov, Nakamura, R., W. Baumjohann, R. A. Treumann, T. L. Zhang, M. Volwerk, Z. Vörös, A. Balogh, K. -H. Glassmeier, B. Klecker, H. Rème, and L. Kistler, “Current Sheet Structure Near Magnetic X-Line Observed by Cluster,” *Geophys. Res. Lett.*, **30**, 33, 2003.
 44. M. A. Shay, J. F. Drake, B. N. Rogers, and R. E. Denton, “Alfvénic Collisionless Magnetic Reconnection and the Hall Term,” *J. Geophys. Res.*, 3759, 2001.
 45. W. M. Farrell, M. D. Desch, M. L. Kaiser, and K. Goetz, “The Dominance of Electron Plasma Waves Near a Reconnection X-Line Region,” *Geophys. Res. Lett.*, **29**, 8, 2002.
 46. S. S. Sazhin, and M. Hayakawa, “Magnetospheric Chorus Emissions: A Review,” *Planet. Space Sci.*, **40**, 681, 1992.
 47. N. P. Meredith, R. B. Horne, and R. R. Anderson, “Substorm Dependence of Chorus Amplitudes: Implications for the Acceleration of Electrons to Relativistic Energies,” *J. Geophys. Res.*, **106**, 13, 165, 2001.
 48. C. F. Kennel and H. E. Petschek, “Limit on Stably Trapped Particle Fluxes,” *J. Geophys. Res.*, **71**, 1, 1966.
 49. M. J. Ledocq, D. A. Gurnett, and G. B. Hospodarsky, *Chorus Source Location from VLF Poynting Measurements with the Polar Spacecraft*.
 50. D. S. Lauben, U. S. Inan, T. F. Bell, and D. A. Gurnett, “Source Characteristics of ELF/VLF Chorus,” *J. Geophys. Res.*, **107**, 1429, doi: 10.1029/2000JA003019, 2002.
 51. M. Parrot, O. Santolik, N. Cornilleau-Wehrin, M. Maksimovic, and C. C. Harvey, “Magnetically Reflected Chorus Waves Revealed by Ray Tracing with Cluster Data,” *Ann. Geophys.*, **21**, 1111, 2003.
 52. N. Cornilleau-Wehrin, P. Chauveau, S. Louis, A. Meyer, J. -M. Nappa, S. Perraut, L. Rézeau, P. Robert, A. Roux, C. de Villedary, Y. de Conchy, L. Friel, C. C. Harvey, D. Hubert, C. Lacombe, R. Manning, F. Wouters, F. Lefeuve, M. Parrot, J. -L. Pinçon, B. Poirier, W. Kofman, Ph. Louarn, and the STAFF Investigator Team, “The Cluster Spatio-Temporal Analysis of Field Fluctuations (Staff) Experiment,” *Space Sci. Rev.*, **107**, 1997.
 53. N. Cornilleau-Wehrin, G. Chanteur, S. Perraut, L. Rézeau, P. Robert, A. Roux, C. de Villedary, P. Canu, M. Maksimovic, Y. de Conchy, D. Hubert, C. Lacombe, F. Lefeuve, M. Parrot, J. -L., Pinçon, P. M. E. Décréau, C. C. Harvey, Ph. Louarn, O. Santolik, H. St. C. Alleyne, M. Roth, T. Chust, O. Le Contel, and STAFF team, “First Results Obtained by the Cluster STAFF Experiment,” *Ann. Geophys.*, **21**, 437, 2003.
 54. U. S. Inan, M. Platino, T. F. Bell, D. A. Gurnett, and J. S. Pickett, “Cluster Measurements of Rapidly Moving Sources of ELF/VLF Chorus,” *J. Geophys. Res.*, **109**, A05214, doi :10.1029/2003JA010289, 2004.
 55. A. Balogh, M. W. Dunlop, S. W. H. Cowley, D. J. Southwood, J. G. Thomlinson, K. H. Glassmeier, G. Musmann, H. Lohr, S. Buchert, M. H. Acuña, D. H. Fairfield, J. A. Slavin, W. Riedler, K. Schwingenschuh, M. G. Kivelson, and the Cluster Magnetometer Team, “The Cluster Magnetic Field Investigation,” *Space Sci. Rev.*, **79**, 65, 1997.

56. A. Balogh, C. M. Carr, M. H. Acuña, M. W. Dunlop, T. J. Beek, P. Brown, K. -H. Fornaçon, E. Georgescu, K. H. Glassmeier, J. Harris, G. Musmann, T. Oddy, and K. Schwingenschuh, "The Cluster Magnetic Field Investigation: Overview of In-Flight Performance and Initial Results," *Ann. Geophys.*, **19**, 1207, 2001.
57. N. Dunkel and R. Helliwell, "Whistler Mode Emissions in the OGO 1 Satellite," *J. Geophys. Res.*, **74**, 6371, 1969.
58. N. Cornilleau-Wehrin, J. Solomon, A. Korth, and G. Kremser, "Experimental Study of the Relationship Between Energetic Electrons and ELF Waves Observed on GEOS: A Support to Quasi-Linear Theory," *J. Geophys. Res.*, **90**, 4141, 1985.
59. M. Parrot, O. Santolik, D. A. Gurnett, J. S. Pickett, and N. Cornilleau-Wehrin, "Characteristics of Magnetospherically Reflected Chorus Waves Observed by Cluster," *Ann. Geophys.*, **22**, 2597, 2004.
60. O. Santolik, D. A. Gurnett, J. S. Pickett, M. Parrot, and N. Cornilleau-Wehrin, "Spatio-Temporal Structure of Storm-Time Chorus," *J. Geophys. Res.*, **108**, 1278, doi:10.1029/2002JA009791, 2003.
61. O. Santolik, D. A. Gurnett, J. S. Pickett, M. Parrot, and N. Cornilleau-Wehrin, "A Microscopic and Nanoscopic View of Storm-Time Chorus on 31 March 2001," *Geophys. Res. Lett.*, **31**, L02801, doi: 10.1029/2003GL018757, 2004.
62. O. Santolik, D. Gurnett, and J. Pickett, "Multipoint Investigation of the Source Region of Storm-Time Chorus," *Ann. Geophys.*, **22**, 2555, 2004.
63. J. -L. Pinçon and U. Motschmann, "Multi-Spacecraft Filtering: General Framework," in G. Paschmann and P. Daly (eds.), *Analysis Methods for Multi-Spacecraft Data*. Bern: ISSI, **65**, 1998.
64. J. -L. Pinçon and F. Lefeuvre, "Local Characterization of Homogeneous Turbulence in a Space Plasma from Simultaneous Measurement of Field Line Components at Several Points in Space," *J. Geophys. Res.*, **96**, 1789, 1991.
65. K. -H. Glassmeier, U. Motschmann, M. Dunlop, A. Balogh, M. H. Acuña, C. Carr, G. Musmann, K. -H. Fornaçon, K. Schweda, J. Vogt, E. Georgescu, and S. Buchert, "Cluster as a Wave Telescope – First Results from the Fluxgate Magnetometer," *Annales Geophysicae*, **19**, 1439, 2001. Correction, ang, 21, 1071, 2003.
66. F. Sahraoui, J. -L. Pinçon, G. Belmont, L. Rézeau, N. Cornilleau-Wehrin, P. Robert, L. Mellul, J. -M., Bosqued, J. -M., A. Balogh, P. Canu, and G. Chanteur, "ULF Wave Identification in the Magnetosheath: The k-Filtering Technique Applied to Cluster II Data," *J. Geophys. Res.*, **108**, 1335, 2003. Correction, *JGR*, **109**, A04222, 2004.
67. S. N. Walker, F. Sahraoui, M. A. Balikhin, G. Belmont, J. -L. Pinçon, L. Rézeau, H. Alleyne, N. Cornilleau-Wehrin, and M. André, "A Comparison of Wave Mode Identification Techniques," *Ann. Geophys.*, **22**, 3021, 2004.
68. P. Robert, A. Roux, C. C. Harvey, M. W. Dunlop, P. W. Daly, and K. H. Glassmeier, "Tetrahedron Geometric Factors," in G. Paschmann and P. Daly (eds.), *Analysis Methods for Multi-Spacecraft Data*, Bern: ISSI, **65**, 1998.
69. P. M. E. Décréau, P. Fergeau, V. Krasnosselskikh, E. Le Guirriec, M. Lévêque, Ph. Martin, O. Randriamboarison, J. -L. Rauch, F. -X. Sené, H. C. Séran, J. -G. Trotignon, P. Canu, N. Cornilleau, H. de Féraudy, H. Alleyne, K. Yearby, P. B. Mørgensen, G. Gustafsson, M. André, D. A. Gurnett, F. Darrouzet, J. Lemaire, C. C. Harvey, P. Travnicek, and Whisper Experimenters, "Early Results from the Whisper Instrument on Cluster: An Overview," *Ann. Geophys.*, **19**, 1241, 2001.
70. H. Rème, J. -M. Bosqued, J. -A. Sauvaud, A. Cros, J. Dandouras, C. Aoustin, J. Bouyssou, Th. Camus, J. Cuvilo, C. Mertz, J. -L. Madle, H. Perrier, D. Romefort, J. Rouzaud, D. d'Uston, E. Moebius, K. Crocker, M. Runoff, L. M. Kistler, M. Popecki, D. Hovestadt, B. Klecker, G. Pashmann, M. Scholer, C. W. Carlson, D. W. Curtis, R. P. Lin, J. P. McFadden, V. Formisano, E. Amata, M. B. Bassano-Cattaneo, P. Baldetti, G. Belluci, R. Bruno, G. Chionchio, A. di Lellis, E. G. Shelley, A. G. Ghielmetti, W. Lennartson, A. Korth, U. Rosenbauer, R. Lundin, S. Olsen, G. K. Parks, M. McCarthy, and H. Balsiger, "The Cluster Ion Spectrometry (CIS) Experiment," *Space Sci. Rev.*, **79**, 303, 1997.
71. K. Rönmark, "WHAMP, Waves in Homogeneous, Anisotropic, Multicomponent Plasmas," *KGI Report 179*, Kiruna Geophysical Institute, 1982.
72. F. Sahraoui, G. Belmont, J. -L. Pinçon, L. Rézeau, A. Balogh, P. Robert, and N. Cornilleau-Wehrin, "Magnetic Turbulent Spectra in the Magnetosheath: New Insights," *Ann. Geophys.*, **22**, 2283, 2004.
73. F. Sahraoui, G. Belmont, and L. Rézeau, "From Bi-Fluid to Hall-MHD Weak Turbulence: Hamiltonian Canonical Formulations," *Physics of Plasma*, **10**, 1335, 2003.
74. Y. Narita, K. -H. Glassmeier, S. Schäfer, U. Motschmann, M. Fränz, I. Dandouras, K. Fornaçon, E. Georgescu, A. Korth, H. Rème, and I. Richter, "Alfvén Waves in the Foreshock Propagating Upstream in the Plasma Rest Frame: Statistics from Cluster Observations," *Ann. Geophys.*, **22**, 2315, 2004.
75. M. A. Balikhin, O. A. Pokhotelov, S. N. Walker, E. Amata, M. André, M. Dunlop, and H. Alleyne, "Minimum Variance Free Wave Identification: Application to Cluster Electric Field Data in the Magnetosheath," *Geophys. Res. Lett.*, **30**, 10, 10.1029/2002GL015871, 2003.
76. T. D. Carozzi, A. M. Buckley, and M. P. Gough, "Instantaneous Local Wave Vector Estimation from Multi-Spacecraft Measurements Using Few Spatial Points," *Ann. Geophys.*, **22**, 2633, 2004.
77. O. D. Constantinescu, K. -H. Glassmeier, R. Treumann, and K. -H. Fornaçon, "Magnetic Mirror Structures Observed by Cluster in the Magnetosheath," *Geophys. Res. Lett.*, **30**, 15, 1802, doi: 10.1029/2003GL017313, 2003.
78. T. S. Horbury, E. A. Lucek, A. Balogh, I. Dandouras, and H. Rème, "Motion and Orientation of Magnetic Field Dips and Peaks in the Terrestrial Magnetosheath," *J. Geophys. Res.*, **109**, A09209, doi: 10.1029/2003JA010237, 2004.
79. J. De Keyser, G. Gustafsson, M. Roth, F. Darrouzet, M. Dunlop, H. Rème, A. Fazakerley, P. Décréau, and N. Cornilleau-Wehrin, "Reconstruction of the Magnetopause and Low Latitude Boundary Layer Topology Using Cluster Multi-Point Measurements," *Ann. Geophys.*, **22**, 2381, 2004.
80. R. Behlke, M. André, S. C. Buchert, A. Vaivads, A. I. Eriksson, E. A. Lucek, and A. Balogh, "Multi-Point Electric Field Measurements of Short Large-Amplitude Magnetic Structures (SLAMS) at the Earth's Quasi-Parallel Bow Shock," *Geophys. Res. Lett.*, **30**, 4, doi: 10.1029/2003GL015871, 2003.
81. M. Maksimovic, S. D. Bale, T. S. Horbury and M. Andre, "Bow Shock Motions Observed with CLUSTER," *Geophysical Research Letters*, **30**, 7, 1393, doi: 10.1029/2002GL016761, 2003.
82. H. Hasegawa, M. Fujimoto, T. -D. Phan, H. Rème, A. Balogh, M. W. Dunlop, C. Hashimoto, and R. TanDokoro, "Rolled-Up Kelvin-Helmholtz Vortices and Associated Solar Wind Entry at Earth's Magnetopause," *Nature*, **430**, 755, 2004.
83. V. Sergeev, A. Runov, W. Baumjohann, R. Nakamura, T. L. Zhang, A. Balogh, Ph. Louarn, J. A. Sauvaud, and H. Rème, "Orientation and Propagation of Current Sheet Oscillations," *Geophys. Res. Lett.*, **31**, L05807, doi: 10.1029/2003GL019346, 2004.
84. M. Volwerk, R. Nakamura, W. Baumjohann, R. A. Treumann, A. Runov, Z. Vörös, T. L. Zhang, Y. Asano, B. Klecker, I. Richter, A. Balogh, and H. Rème, "A Statistical Study of Compressional Waves in the Tail Current Sheet," *J. Geophys. Res.*, **108**, SMP12-1, doi: 10.1029/2003JA010155, 2003.
85. O. Alexandrovna, A. Mangeney, M. Maksimovic, C. Lacombe, N. Cornilleau-Wehrin, E. A. Lucek, P. M. E. Décréau, J. -M. Bosqued, P. Travnicek, and A. N. Fazakerley, "Cluster Observations of Finite Amplitude Alfvén Waves and Small Scale Magnetic Filaments Downstream of a Quasi-Perpendicular Shock," *J. Geophys. Res.*, **109**, A05207, doi: 10.1029/2003JA010056, 2004.

86. K. Stasiewicz, M. Longmore, S. Buchert, P. K. Shukla, B. Lavraud, and J. Pickett, "Properties of Fast Magnetosonic Shocklets at the Bow Shock," *Geophys. Res. Lett.*, **30**, 2241, doi: 10.1029/2003GL017971, 2003.
87. Z. Vörös, W. Baumjohann, R. Nakamura, A. Runov, M. Volwerk, T. L. Zhang, and A. Balogh, "Wavelet Analysis of Magnetic Turbulence in the Earth's Plasma Sheet," *Phys. Plasmas*, **11**, 1333, 2004.
88. K. Sigsbee, C. Kletzing, D. Gurnett, J. Pickett, A. Balogh, and E. Lucek, "Statistical Behaviour of Foreshock Langmuir Waves Observed by the Cluster Wideband Data Plasma Wave Receiver," *Ann. Geophys.*, **22**, 2337, 2004.
89. K. Sigsbee, C. Kletzing, D. Gurnett, J. Pickett, A. Balogh, and E. Lucek, "The Dependence of Langmuir Wave Amplitudes on Position in the Earth's Foreshock," *Geophys. Res. Lett.*, **31**, L07805, doi: 10.1029/2004GL019413, 2004.
90. J. Blecki, S. Savin, N. Cornilleau-Wehrin, K. Kossacki, M. Parrot, H. Rothkaehl, K. Stasiewicz, R. Wronowski, O. Santolik, and J. -A. Sauvaud, "Fine Structure of the Polar Cusp as Deduced from the Plasma Wave and Plasma Measurements," *Adv. Space Res.*, **32**, 3, 315, 2003.
91. O. Santolik, F. Nemeč, K. Gereová, E. Macúsová, Y. de Conchy, and N. Cornilleau-Wehrin, "Systematic Analysis of Equatorial Noise Below the Lower Hybrid Frequency," *Ann. Geophys.*, **22**, 2587, 2004.
92. A. Masson, U. Inan, H. Laakso, O. Santolik, and P. Décréau, "Cluster Observations of Mid-Latitude Hiss Near the Plasmopause," *Ann. Geophys.*, **22**, 2004.
93. K. Stasiewicz, P. K. Shukla, G. Gustafsson, S. Buchert, B. Lavraud, B. Thidé, and Z. Klos, "Slow Magnetosonic Solitons Detected by the Cluster Spacecraft," *Phys. Rev. Lett.*, **30**, 2241, doi: 10.1029/PhysRevLett.90.085002, 2003.
94. J. Pickett, L. Chen, S. Kahler, O. Santolik, D. Gurnett, B. Tsurutani, and A. Balogh, "Isolated Electrostatic Structures Observed Throughout the Cluster Orbit: Relationship to Magnetic Field Strength," *Ann. Geophys.*, **22**, 2515, 2004.
95. C. Mazelle, K. Meziane, D. Le Quéau, M. Wilber, J. P. Eastwood, H. Rème, J. -A. Sauvaud, J. -M. Bosqued, I. Dandouras, M. McCarthy, L. M. Kistler, B. Klecker, A. Korth, M. B. Bavassano-Cattaneo, G. Pallochia, R. Lundin, and A. Balogh, "Production of Gyrating Ions from Nonlinear Wave-Particle Interaction Upstream from the Earth's Bow Shock: A Case Study from Cluster-CIS," *Planet. Space Sci.*, **51**, 785, 2003.
96. ftp://ftp.rssd.esa.int/pub/Cluster/Publications/Cluster_publications.htm, Cluster scientific papers.
97. J. D. Menietti, R. R. Anderson, J. S. Pickett, D. A. Gurnett, and H. Matsumoto, "Near-Source and Remote Observations of Kilometric Continuum Radiation from Multi-Spacecraft Observations," *J. Geophys. Res.*, **108**, A11, 1393, doi: 10.1029/2003JA009826, 2003.
98. P. Décréau, C. Ducoin, G. Le Rouzic, O. Randriamboarison, J. -L. Rauch, J. -G. Trotignon, X. Vallières, P. Canu, F. Darrouzet, P. Gough, A. Buckley, and T. Carozzi, "Observation of Continuum Radiations from the Cluster Fleet: First Results from Direction Finding," *Ann. Geophys.*, **22**, 2607, 2004.
99. L. J. C. Woolliscroft, H. St. C. Alleyne, C. M. Dunford, A. Sumner, J. A. Thompson, S. N. Walker, K. H. Yearby, A. Buckley, S. Chapman, M. P. Gough, and The DWP Co-Investigators, "The Digital Wave-Processing Experiment on Cluster," *Space Sci. Rev.*, **79**, 1997, pp. 209–231.